Copy 5
RM E52A31

NACA RM E52A31

NACA

RESEARCH MEMORANDUM

SOME EFFECTS OF CHANGING SOLIDITY BY VARYING THE NUMBER OF BLADES ON PERFORMANCE OF AN AXIAL-FLOW COMPRESSOR STAGE

By Raymond M. Standahar and George K. Serovy

Lewis Flight Propulsion Laboratory
Cleveland, Ohio

NATIONAL ADVISORY COMMITTEE
FOR AERONAUTICS

WASHINGTON
April 14, 1952

NATIONAL ADVISORY COMMITTEE FOR AERONAUTICS

RESEARCH MEMORANDUM

SOME EFFECTS OF CHANGING SOLIDITY BY VARYING THE NUMBER OF BLADES ON PERFORMANCE OF AN AXIAL-FLOW COMPRESSOR STAGE

By Raymond M. Standahar and George K. Serovy

SUMMARY

An investigation was conducted to determine some of the basic problems and effects involved in a change of solidity accomplished by a change in the number of blades in an axial-flow-compressor rotor row and in a complete stage.

A complete stage designed to obtain a high total-pressure ratio by combining high blade loading and high relative inlet Mach number was installed in a 14-inch-tip-diameter compressor with a hub-tip diameter ratio of 0.8 at the rotor leading edge. The stage was designed using 44 rotor blades (solidity of 1.50 at mean radius) and 46 stator blades (solidity = 1.56 at mean radius). Performance of rotors containing 44, 30, and 22 of the original rotor blades (mean radius solidities of 1.50, 1.02, and 0.75, respectively) was determined with no stator blades installed, and performance of the stage with half of the rotor and stator blades removed was obtained for comparison with previously reported results of an investigation of the complete high-solidity stage.

Rotor data for a range of corrected weight flows at each of five equivalent tip speeds from 669 to 962 feet per second indicated that peak pressure ratio for a given speed was higher and was obtained at a lower weight flow as solidity was increased. The peak efficiencies for the three rotor solidities investigated were nearly equal at a given speed and occurred at lower weight flows as solidity was increased.

Complete stage data showed that secondary flows produced a large high-loss region near the hub behind the low-solidity stator blades. A large reduction in the size and severity of this loss region for the high-solidity stage indicated that the secondary flows producing this loss were reduced by increasing stator solidity.

INTRODUCTION

From both manufacturing cost and weight considerations, it is desirable to design multistage axial-flow compressors using the minimum number of blades necessary to give the required performance. One method of reducing the number of blades required is to increase the pressure ratio per stage so that the design over-all pressure ratio can be obtained with fewer stages, and a considerable amount of effort has been directed toward this objective. The second method of reducing the number of blades would involve the design of stages which will produce a given stage pressure ratio using lower solidities (chord divided by blade spacing). A complete investigation of the effect of solidity on performance of a compressor stage would require the design of a number of stages using the same design velocity diagrams, but using different combinations of solidity and camber to obtain the required turning angles through the rotor and stator. It would also be necessary to determine the effect of solidity on performance of stages having various types of flow distribution through the stage. This, obviously, would be an extensive program. A simpler, but less rigorous approach to the problem can be made by changing the solidity of a given stage by changing the number of blades. In this type of investigation, each solidity is essentially a different stage design since no attempt is made to maintain the original design conditions by changing blade camber as solidity is changed. It was believed, however, that such an investigation would be of value in indicating the extent to which cascade data can be used to predict the performance of blade sections at different solidities, and that some knowledge of the variation of efficiency and range of operation of blade sections with solidity would be obtained.

In order to study some of these basic effects of a change of solidity, a compressor stage designed to obtain a high total-pressure ratio by combining high blade loading and high relative inlet Mach number was installed in a 14-inch-tip-diameter compressor with a hub-tip diameter ratio of 0.8 at the rotor leading edge (reference 1). The stage was designed using 44 rotor blades (solidity, $\sigma = 1.50$ at mean radius) and 46 stator blades ($\sigma = 1.56$ at mean radius). In the first phase of the investigation, the performance of the 44-blade rotor and of rotors containing 30 and 22 of the original blades was determined. This variation in the number of blades gave rotor mean radius solidities of 1.50, 1.02, and 0.75. No stator blades were used in this phase.

Next, to investigate additional solidity effects which might be present in a complete stage, the performance of the stage (inlet guide vanes, rotor, and stator blades) was determined with half of the rotor

and stator blades removed and a comparison was made with the performance of the high-solidity stage reported in reference 1.

Performance curves are presented which show the variation of total-pressure ratio and adiabatic efficiency with corrected weight flow for the three rotors at five equivalent tip speeds from 669 to 962 feet per second. Comparison of the trends of these curves is made with those predicted from two-dimensional cascade data, and blade element data are presented for the rotor tests to facilitate detailed analysis of the results. Rotor results are compared with complete stage data for design solidity and one-half design solidity at the design speed.

SYMBOLS

The following symbols are used in this report:

c	blade chord (ft)
c_p	specific heat at constant pressure (Btu/(lb)($^\circ$F))
J	mechanical equivalent of heat (778 ft-lb/Btu)
P	total pressure (lb/ft^2 absolute)
p	static pressure (lb/ft^2 absolute)
r	radius (ft)
r/r_t	radius ratio
S	blade spacing (ft)
T	total temperature ($^\circ$R)
U	blade velocity at any radius r (ft/sec)
$U_t/\sqrt{\theta}$	equivalent tip speed corrected to standard NACA sea-level conditions (ft/sec)
V	absolute air velocity (ft/sec)
V'	air velocity relative to rotor (ft/sec)
W	weight flow (lb/sec)

$\frac{W\sqrt{\theta}}{\delta}$ weight flow corrected to standard NACA sea-level conditions (lb/sec)

α angle of attack (deg)

β absolute stagger angle, angle between compressor axis and absolute air velocity (deg)

β' relative stagger angle, angle between compressor axis and relative air velocity (deg)

$\Delta\beta$ turning angle of stator (deg)

$\Delta\beta'$ relative turning angle of rotor (deg)

γ ratio of specific heats (1.3947 for normal air)

δ ratio of inlet total pressure to standard NACA sea-level pressure

η_{ad} adiabatic efficiency

θ ratio of inlet total temperature to standard sea-level temperature

ρ density (lb/cu ft)

σ blade element solidity, ratio of chord length to distance between adjacent blades

φ included angle of circular arc (deg)

Subscripts:

av average

e referred to equivalent constant axial-velocity diagram

h hub

m referred to vector mean velocity

max maximum

t tip

u	tangential
z	axial
0	inlet measuring station
1	after guide vane measuring station
2	after rotor measuring station
3	after stator measuring station

APPARATUS AND PROCEDURE

Compressor Design

The assumptions used in the design of the high-solidity compressor stage are given in reference 1. The guide vanes were variable-chord, circular-arc, sheet-metal vanes and were designed by use of the following equation (reference 2):

$$\Delta\beta = \varphi\left(1 - 0.26\sqrt{\frac{s}{c}}\right)$$

The NACA 65-series blower-blade sections with a 6-percent maximum thickness were used for the rotor and stator blades. Rotor blade cambers and angles of attack were selected from the design values of references 3 and 4 to give the flattest pressure distribution for the desired turning angle. In utilizing the design values of references 3 and 4, it was necessary to use an equivalent constant axial velocity diagram based on the mean of the entrance and exit axial velocities (fig. 1). Because the change in stator-blade turning angle with radius was very small, a constant camber section with camber and angle of attack for the flattest pressure distribution at the mean radius section was used.

The high-solidity stage consisted of 40 guide vanes, 44 rotor blades, and 46 stator blades. A summary of the blade design data is presented in table I.

For the rotor solidity tests, rotors containing 44, 30, and 22 blades were used. Rotor mean radius solidities were 1.50, 1.02, and 0.75, respectively. Blade profiles and angle settings were identical with those of the high-solidity blading. No stator blades were installed.

[redacted]

In the investigation of the low-solidity stage, 22 rotor blades and 23 stator blades were installed giving mean radius solidity values of 0.75 for the rotor and 0.78 for the stator. Because of the anticipated decrease in turning through the rotor, the stator blade setting angles (angle between chord line and compressor axis) were arbitrarily reduced 5° in an attempt to keep the blades in a good operating range.

The blades were installed in a compressor having a tip diameter of 14 inches and a hub-tip diameter ratio of 0.8 at the rotor leading edge. The inner-wall profile was designed from continuity of mass flow using constant average axial velocity across the rotor, an isentropic compression process, and the design assumptions of the high-solidity stage.

A schematic diagram of the compressor installation is shown in figure 2. Air was drawn from the test cell through a thin plate orifice which was mounted on the end of an orifice tank and then through a motor-operated butterfly inlet valve into a depression tank (4-ft diameter and 6-ft length). A series of screens, filter paper, and a 3- by 3-inch honeycomb were used in the depression tank to obtain smooth uniform flow into the bellmouth inlet of the compressor. The air was discharged from the compressor collector into the laboratory exhaust system. A motor-driven butterfly valve in the outlet ducting controlled the air flow. A 400-horsepower, 20,000-rpm dynamometer was used to drive the compressor.

Test Procedure

Each rotor configuration was tested over a range of weight flows at equivalent tip speeds of 669, 753, 836, 920, and 962 feet per second, which corresponded to 80, 90, 100, 110, and 115 percent of the high-solidity-stage design speed, respectively. Data for the complete low-solidity stage were taken only at an equivalent tip speed of 836 feet per second. At each speed, the weight flow was varied from the maximum obtainable to a point of audible surge or noticeable blade stall, whichever came first. The following table gives the speed range of the various configurations:

Solidity at mean radius			Equivalent tip speeds (ft/sec)				
Guide Vanes	Rotor	Stator	669	753	836	920	962
1.765	1.50	None	(a)	(a)	(a)	(a)	(a)
1.765	1.02	None	(a)	(a)	(a)	(a)	(a)
1.765	0.75	None	(a)	(a)	(a)	(a)	(a)
1.765	1.50	1.56	(b)	(b)	(b)	(b)	(b)
1.765	0.75	0.78	---	---	(a)	---	---

[a]Present investigation.
[b]Data of reference 1.

Instrumentation

Instrumentation was provided in the depression tank and at the compressor outlet to measure over-all performance and between blade rows to measure individual blade-row performance (see fig. 2). Radial surveys were made after each blade row using four radial positions located at the centers of four equal-annulus-area increments. Preliminary circumferential surveys were made in order to locate the survey instruments so that they were removed from the wakes of upstream blades and instruments.

Temperatures in the depression tank were measured by four thermocouple probes, each containing four iron-constantan thermocouples. Two wall pressure taps were used for pressure measurement. Pressures and temperatures in the tank were assumed to be stagnation values because of the low velocities in the tank.

At station 1 located approximately 1/4 chord length upstream of the rotor blades, measurements were made of the total pressure, static pressure, and flow angle at the four radial positions. As the total temperatures were constant across the guide vanes, no temperature measurements were made at station 1. Total pressure and flow angle were measured with a combination claw total-pressure probe (fig. 3(a)), and static pressure was measured with a wedge-type static-pressure probe (fig. 3(b)). Similar survey instrumentation was used at station 2

(0.2 chord length downstream of the rotor) and station 3 (0.9 chord length downstream of the stator blades). For the runs with stator blades, the total pressure at station 3 was obtained by averaging the readings from a 25-tube circumferential rake (fig. 3(c)), which covered a complete blade passage. Compressor-outlet temperature measurements were made at station 3 using four 4-tip thermocouple rakes (fig. 3(d)). The thermocouples were connected differentially with those at station 0 so that a circumferentially averaged value of the temperature rise across the compressor could be calculated for each of the four radial measuring stations. Compressor instrumentation is summarized in table II.

Air flow through the compressor was measured with a standard thin-plate orifice mounted on the end of an orifice tank. Compressor speed was measured with a precision-type electronic tachometer.

Method of Calculation

The total-pressure ratio used was obtained from a mass-flow-weighted average of the isentropic power input integrated across the flow passage (reference 5).

The adiabatic efficiency used in evaluating compressor performance was calculated from a mass-flow-weighted average of the total-temperature rise across the compressor and a mass-flow-weighted average of the isentropic power input (reference 5):

$$\left(\frac{P_3}{P_0}\right)_{av} = \left\{ \frac{\frac{2\pi J c_p}{550} \int_{r_{h,3}}^{r_{t,3}} \rho_3 V_{z,3} r_3 T_0 \left[\left(\frac{P_3}{P_0}\right)^{\frac{\gamma-1}{\gamma}} - 1 \right] dr}{\frac{2\pi J c_p T_0}{550} \int_{r_{h,3}}^{r_{t,3}} \rho_3 V_{z,3} r_3 \, dr} + 1 \right\}^{\frac{\gamma}{\gamma-1}}$$

$$\eta_{ad} = \frac{\frac{2\pi J c_p}{550} \int_{r_{h,3}}^{r_{t,3}} \rho_3 V_{z,3} r_3 T_0 \left[\left(\frac{P_3}{P_0}\right)^{\frac{\gamma-1}{\gamma}} - 1 \right] dr}{\frac{2\pi J c_p}{550} \int_{r_{h,3}}^{r_{t,3}} \rho_3 V_{z,3} r_3 (T_3 - T_0) \, dr}$$

[redacted]

RESULTS AND DISCUSSION

Rotor Performance

Pressure ratio and adiabatic efficiency. - Total-pressure ratio and adiabatic efficiency are plotted in figure 4 against corrected weight flow for the three rotor solidities at five equivalent tip speeds from 669 to 962 feet per second. Weight-flow limitations in the test compressor downstream of the blading made it impossible to operate the rotors over part of the high-weight-flow region of their operating range.

The peak total-pressure ratio increased with solidity at all speeds, and at any given speed the peak-pressure-ratio point shifted toward lower weight flows as solidity increased. The change in pressure ratio with solidity was greatest at the low weight flows and the curves converged at increasing values of the weight flow. These are trends that could be predicted from two-dimensional cascade results. Figure 5 shows the variation of turning angle with angle of attack for an NACA 65-(18)10 airfoil at a constant inlet stagger angle of 45° (from the two-dimensional cascade data of reference 6). Curves are plotted for cascade solidities of 0.75, 1.00, and 1.50, which correspond to the mean radius solidities of the three rotors tested. Inlet stagger angles at constant rotor speed change with flow so that the curves of figure 5 are not directly applicable to compressor data but they are sufficiently accurate for use in indicating trends. For a constant equivalent tip speed, a given compressor corrected weight flow corresponds to a constant blade angle of attack, and angle of attack increases as weight flow decreases. In figure 5, at high angles of attack which correspond to low compressor flows, turning angle increases with solidity. Because pressure ratio is a function of turning angle, higher peak pressure ratios were obtained with the high-solidity rotor. The peak turning is obtained at higher angles of attack as solidity increases. This explains the movement of the peak pressure ratio to lower weight flows as rotor solidity increased at a constant speed. At low cascade angles of attack, which correspond to high compressor weight flows, the turning-angle curves for the three solidities converge in a manner similar to the pressure-ratio curves for the three rotor solidities.

The variation of efficiency with solidity for the compressor cannot be readily predicted from cascade data. The adiabatic efficiency curves of figure 4 show that the peak values of efficiency for all three rotor solidities were approximately the same for a given equivalent tip speed. The weight flow at which the peak value occurred decreased with increasing solidity at a given speed. The decreased

efficiency at low weight flow was due to the increase in losses caused by blade stall and separation. The effect of solidity on the weight flow range for good efficiency could not be determined because of the previously mentioned compressor flow limitation.

Variation of peak pressure ratio with solidity. - The variation of peak pressure ratio and the corresponding adiabatic efficiency with equivalent tip speed are indicated in figure 6 for the three rotor solidities. The maximum relative inlet Mach number represented by these curves was approximately 0.8. These curves show that it should be possible to design a low-solidity stage which would produce a relatively high total-pressure ratio with good efficiency by increasing the relative Mach number and using blade cambers of the same order used in the original stage design of the investigation. The same result could probably be attained using low solidity, higher cambers, and relative inlet Mach numbers no higher than used in the design of the stage of this investigation. It should be remembered that critical Mach numbers are lower for highly cambered sections if the inlet angle, angle of attack, and solidity are held constant. These factors may limit the use of highly cambered, low-solidity blades to low inlet Mach numbers if the operating range of angle of attack is expected to be reasonably wide.

Blade element performance. - Rotor performance on a blade element basis is presented in figures 7 to 10. Rotor angle of attack, turning angle, total-pressure ratio, adiabatic efficiency, relative inlet Mach number, inlet stagger angle, axial velocity ratio, and corrected inlet axial velocity for an equivalent tip speed of 836 feet per second are plotted against corrected weight flow for the three rotor solidities. The variation of each of the quantities is given for the four radial measuring stations (see table II).

As weight flow was reduced, which increased the blade angle of attack, the turning angle for the blade region near the tip was the first to break down (see fig. 7). The break in the turning angle curve for this blade region moved to higher weight flows as solidity was decreased. Another result of the breakdown in flow near the tip can be seen in figure 9. The axial velocity ratio across the rotor in the tip region dropped sharply as weight flow was decreased. This drop is a direct result of passage blockage due to flow separation, and a result of the requirements of equilibrium of high static pressures, even with low total pressures. Further effects of the tip-region stall were decreases in both pressure ratio and adiabatic efficiency as shown in figure 8. The maximum tip-section efficiency decreased slightly with solidity, and the spread between the hub and tip section efficiencies increased with decreasing solidity. This change in element efficiency has very little effect on computed over-all efficiency,

which is a mass-flow-weighted average, because of a radial shift in discharge weight flow.

The flow distribution at the rotor inlet was unaffected by changes in solidity or by the breakdown of flow at the rotor tip for this 0.8 hub-tip ratio stage. This is indicated by comparison of the relative inlet Mach number and stagger angle plots of figure 10.

Cascade comparison. - Rotor equivalent turning angles are compared in figure 11 with those predicted from two-dimensional cascade data. For each rotor solidity, equivalent turning angle is plotted against radius ratio for a data point near peak efficiency at an equivalent tip speed of 836 feet per second. Measured inlet conditions and the cascade data of reference 6 were used to predict rotor turning angles which are also plotted against radius ratio. Observed rotor turning angles over most of the passage were lower than the predicted cascade values. Near the outer wall there was a tendency toward overturning in the rotor row, but there was no consistent variation with solidity of the magnitude of the difference between rotor and cascade data.

The reasons for the difference between cascade predicted turning angle and rotor turning angles shown in figure 11 are difficult to isolate. Deviations from two-dimensional flow in the compressor, especially near the inner and outer walls, are partly responsible. Variations in the axial velocity ratio also contribute to the difference, although the use of equivalent turning angle is an attempt to minimize this effect. The cascade data of reference 6 are for a 10-percent-chord thick airfoil, while the rotor blades used were of 6 percent thickness. Reference 7 indicates that the differences between rotor and cascade data would be increased by not more than 0.5° if the cascade data were for a 6-percent-chord thick section. This leads to an apparent inconsistency between the result presented in reference 1 and the comparison of figure 11. For the design point shown in figure 2 of reference 1, the experimental total-pressure ratio is higher than the calculated total-pressure ratio. This would indicate higher rotor turning angles than the cascade design values. Figure 11 shows measured rotor turning angles which are, in general, lower than those predicted from reference 6. It should be noted that this inconsistency is a result of differences between the extrapolated cascade data used in the original stage design and the data of reference 6 and does not affect the accuracy of the experimental data of reference 6 or of this report.

Complete Stage Performance

Pressure ratio and adiabatic efficiency. - The performance is compared in figure 12 at an equivalent rotor tip speed of 836 feet per second of the complete high-solidity stage, the same stage with half

of the rotor and stator blades removed, the high-solidity rotor, and the same rotor with half of the blades removed. The high-solidity stage data are taken from reference 1. Stator blade setting angles measured with respect to the compressor axis for the low-solidity stage were decreased 5° in an attempt to improve blade-row matching.

Good agreement was obtained between the data for the high-solidity stage and those for the rotor. This indicates good matching of the rotor and stator rows and a low loss in the stator blade row. There was, however, a large difference between the stage and rotor results for the low-solidity tests. Both efficiency and total-pressure ratio were lower for the data with stators over the entire range covered, indicating a poor match between the rotor and stator rows or serious secondary flow losses in the low-solidity stator blade row, or both.

Stator-blade losses. - In order to determine whether there were large stator blade losses in the low-solidity stage, a close examination of the available data was made. The results of total-pressure-rake surveys after the stator blade row are shown in figure 13. Figure 13(a) shows the circumferential variation of a total-pressure deficiency parameter for six radial stations at a corrected weight flow of 14.1 pounds per second (approximately maximum efficiency). Losses in the blade wake were not excessive, but a large high-loss region occured in the center of the blade passage near the hub (positions D and D_1). Figures 13(b) and 13(c) are similar plots for weight flows of 12.4 and 10.0 pounds per second, respectively. Increased blade wakes for these low weight flows were the result of flow separation from the blade surface. This loss region has been found in previous investigations of axial-flow compressors and is probably caused by secondary flow interacting with rotating hub boundary layer (reference 8). Only a small part of the total mass flow is affected by the loss region because of a radial shift in flow toward the outer wall of the passage. This shift is shown in figures 14 and 15, which are plots of the radial distribution of flow before and after the stator blades. For this reason, the entire difference between the performance of the low-solidity stage and the low-solidity rotor should not be charged to the stator blade secondary flow losses, as a considerable part of the difference is undoubtedly due to mismatching of the rotor and stator rows.

For comparison, figure 16 shows total-pressure wake surveys after the high-solidity stage stator blades. Weight flows were approximately equal to those of figure 13. Only four radial measuring stations were used. These curves show that the magnitude of the secondary flows causing the high-loss region near the hub can be reduced by increasing solidity. It may be desirable to maintain higher solidities in compressor design in order to minimize these losses, which would certainly have an effect on the flow distribution in succeeding stages.

SUMMARY OF RESULTS

An investigation was conducted to determine some of the basic problems and effects involved in a change of solidity in an axial-flow compressor rotor row and in a complete stage. From this investigation, in which the solidity of a given blade design was varied by changing the number of blades, the following results were obtained:

1. Peak pressure ratio for a given equivalent tip speed was higher and was obtained at a lower weight flow as solidity increased. The variation in pressure ratio between solidities was reduced by increasing weight flow (decreasing rotor angle of attack) at a given speed. These trends were in agreement with those predicted from two-dimensional cascade results.

2. For the same equivalent tip speed, the peak efficiencies of each of the three rotor solidities investigated were very nearly equal and occurred at a lower weight flow as solidity was increased.

3. Rotor equivalent turning angles were lower than those predicted by cascade results over the major portion of the compressor passage.

4. Complete stage data indicated that secondary flows produced a large high-loss region near the hub behind stator blades with a mean radius solidity of 0.78. The size and the severity of this loss region were greatly reduced for a blade solidity of 1.56.

Lewis Flight Propulsion Laboratory
National Advisory Committee For Aeronautics
Cleveland, Ohio

REFERENCES

1. Voit, Charles H., Guentert, Donald C., and Dugan, James F.: Effect of Mach Number on Over-All Performance of Single-Stage Axial-Flow Compressor Designed for High Pressure Ratio. NACA RM E50D26, 1950.

2. Howell, A. R.: The Present Basis of Axial Flow Compressor Design. Part I. Cascade Theory and Performance. R & M No. 2095, British A.R.C., June 1942.

3. Bogdonoff, Seymour M., and Bogdonoff, Harriet E.: Blade Design Data for Axial-Flow Fans and Compressors. NACA ACR L5F07a, 1945.

[redacted]

4. Bogdonoff, Seymour M.: N.A.C.A. Cascade Data for the Blade Design of High-Performance Axial-Flow Compressors. Jour. Aero. Sci., vol. 15, no. 2, Feb. 1948, pp. 89-95.

5. Mankuta, Harry, and Guentert, Donald C.: Investigation of Performance of Single-Stage Axial-Flow Compressor Using NACA 5509-34 Blade Section. NACA RM E8F30, 1948.

6. Herrig, L. Joseph, Emery, James C., and Erwin, John R.: Systematic Two-Dimensional Cascade Tests of NACA 65-Series Compressor Blades at Low Speeds. NACA RM L51G31, 1951.

7. Herrig, L. Joseph, Emery, James C., and Erwin, John R.: Effect of Section Thickness and Trailing-Edge Radius on Performance of NACA 65-Series Compressor Blades in Cascade at Low Speeds. NACA RM L51J16, 1951.

8. Carter, A. D. S.: Three Dimensional Flow Theories for Axial Compressors and Turbines. Rep. R. 37, British N.G.T.E., Sept. 1948.

[redacted]

TABLE I - BLADE DESIGN DATA

Guide vane (40 blades)			
	Hub	Mean	Tip
Radius ratio, leading edge	0.747	0.906	1.000
Included angle, deg	19.3	23.9	26.8
Incident angle, deg	0	0	0
Chord, in.	1.43	1.76	1.97
Blade thickness, in.	0.06	0.06	0.06
Solidity	1.74	1.765	1.790
Blade section	Circular arc, 4.25 in. radius		
Rotor blade (44 blades)			
	Hub	Mean	Tip
Radius ratio, leading edge	0.800	0.906	1.000
Turning angle, deg	39.7	31.2	23.4
Angle of attack, deg	25.6	18.7	15.7
Relative inlet Mach number	0.668	0.704	0.740
Inlet-air stagger angle, deg	45.0	49.1	52.8
Chord, in.	1.35	1.35	1.35
Solidity	1.69	1.50	1.35
Blade section	65-(20.8)06	65-(16.0)06	65-(13.1)06
Stator blade (46 blades)			
	Hub	Mean	Tip
Radius ratio, leading edge	0.832	0.906	1.000
Turning angle, deg	31.2	30.7	29.5
Angle of attack, deg	17.4	16.75	15.8
Absolute inlet Mach number	0.734	0.702	0.664
Stagger angle, deg	47.2	47.7	49.1
Chord, in.	1.35	1.35	1.35
Solidity	1.69	1.56	1.41
Blade section	65-(13.8)06	65-(13.8)06	65-(13.8)06

[redacted]

TABLE II - INSTRUMENTATION

Station	Radial measuring position		Measurement	Instrument	Circumferential positions
	Station	Distance (in.)			
Inlet tank, 0			Total pressure	Wall taps	2
			Total temperature	Thermocouple probe	4
After guide vanes, 1	A	6.836	Total pressure and flow angle	Claw total-pressure probe	1
	B	6.494			
	C	6.136	Static pressure	Wedge-type static-pressure probe	1
	D	5.754			
				Outer wall taps	5
After rotor blades, 2	A	6.861	Total pressure and flow angle	Claw total-pressure probe	1
	B	6.573			
	C	6.273	Static pressure	Wedge-type static-pressure probe	1
	D	5.958			
				Outer wall taps	5
				Inner wall taps	2
After stator blades, 3	[a]A_1	6.932	Total pressure	25-Tube total-pressure rake	1
	A	6.890	Flow angle	Claw total-pressure probe	1
	B	6.662	Static pressure	Wedge-type static-pressure probe	1
	C	6.428			
	D	6.185		Outer wall taps	5
	[a]D_1	6.128			
				Inner wall taps	2
			Total temperature	4-Tip thermocouple probe	4

[a]Total pressure rake only.

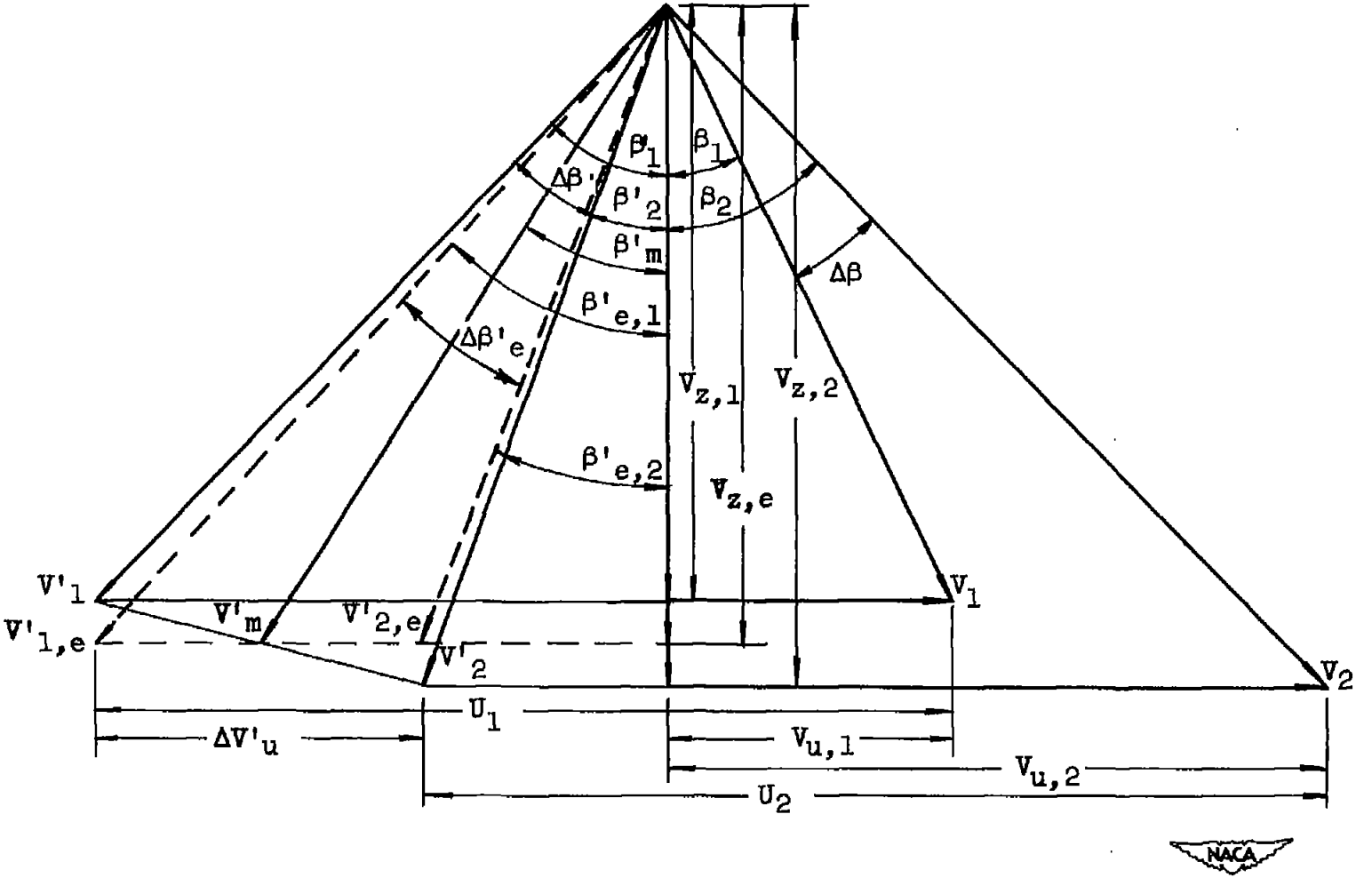

Figure 1. - Typical variable axial-velocity diagram with equivalent values shown as dotted lines.

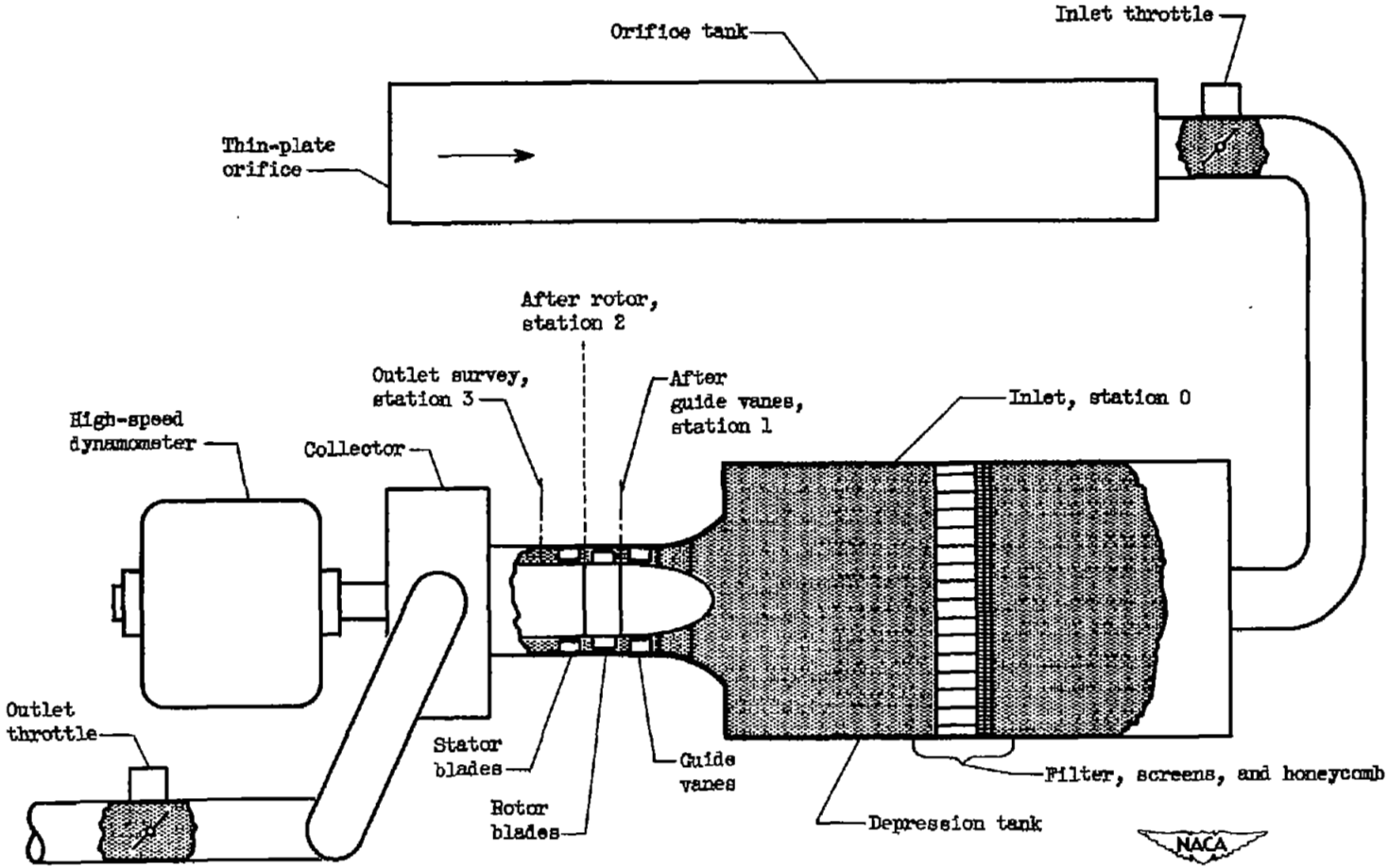

Figure 2. - Schematic diagram of compressor installation.

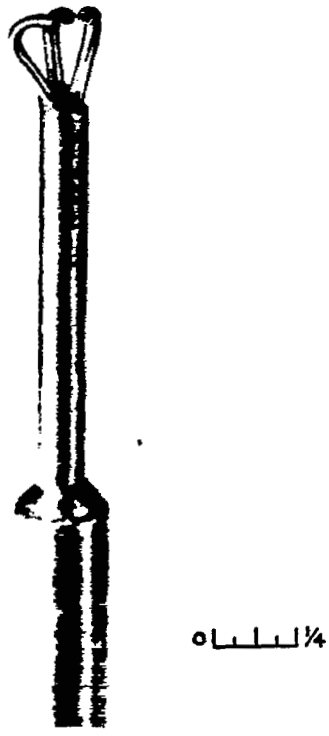

(a) Combination total-pressure probe.

(b) Wedge-type static-pressure probe.

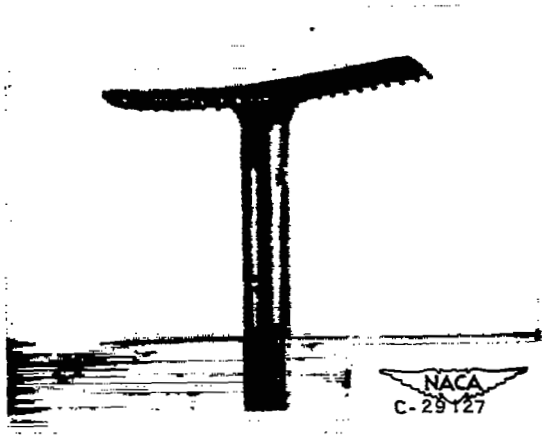

(c) Total-pressure rake.

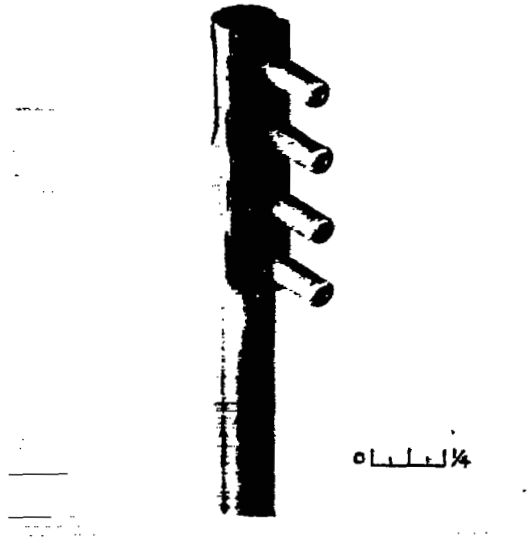

(d) Thermocouple rake.

Figure 3. - Instrumentation.

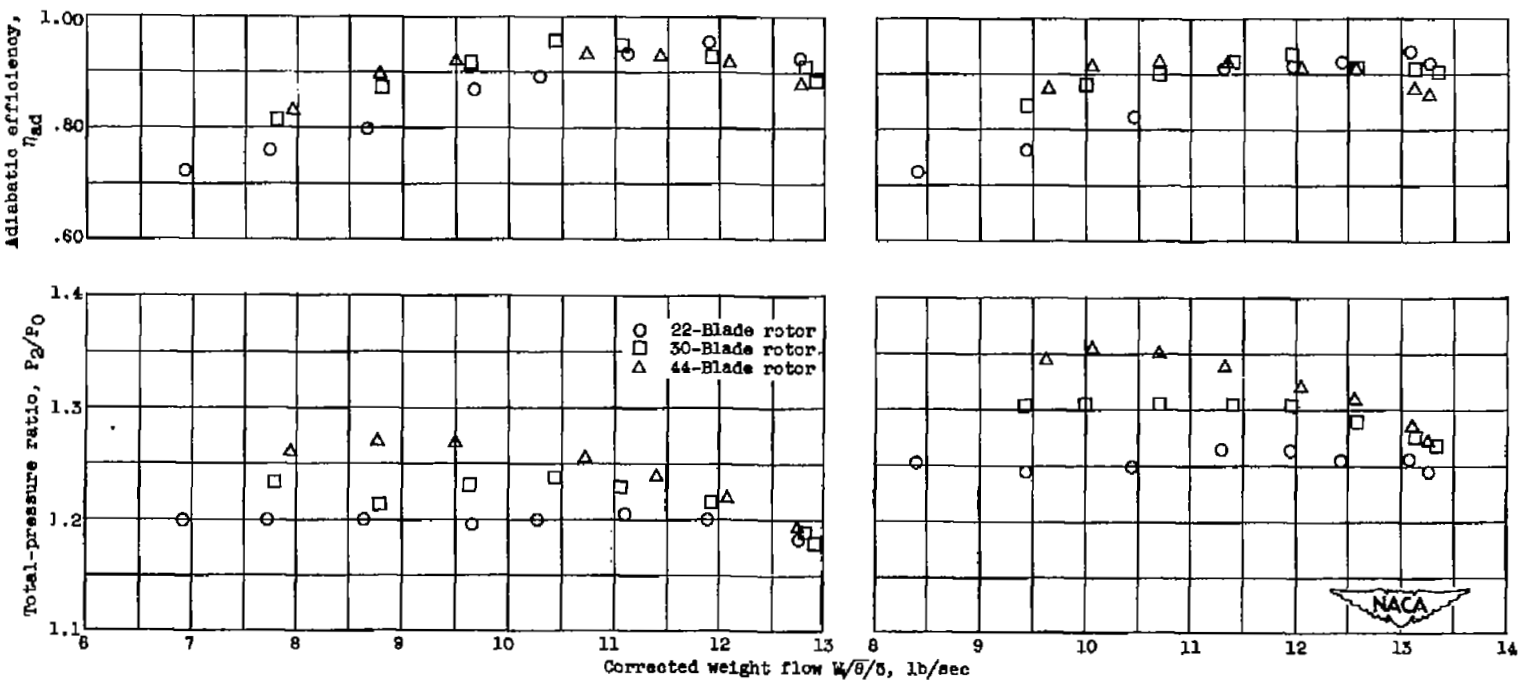

(a) Equivalent tip speed, 669 feet per second.

(b) Equivalent tip speed, 753 feet per second.

Figure 4. - Variation of total-pressure ratio and adiabatic efficiency with corrected weight flow.

(c) Equivalent tip speed, 838 feet per second.

(d) Equivalent tip speed, 920 feet per second.

Figure 4. - Continued. Variation of total-pressure ratio and adiabatic efficiency with corrected weight flow.

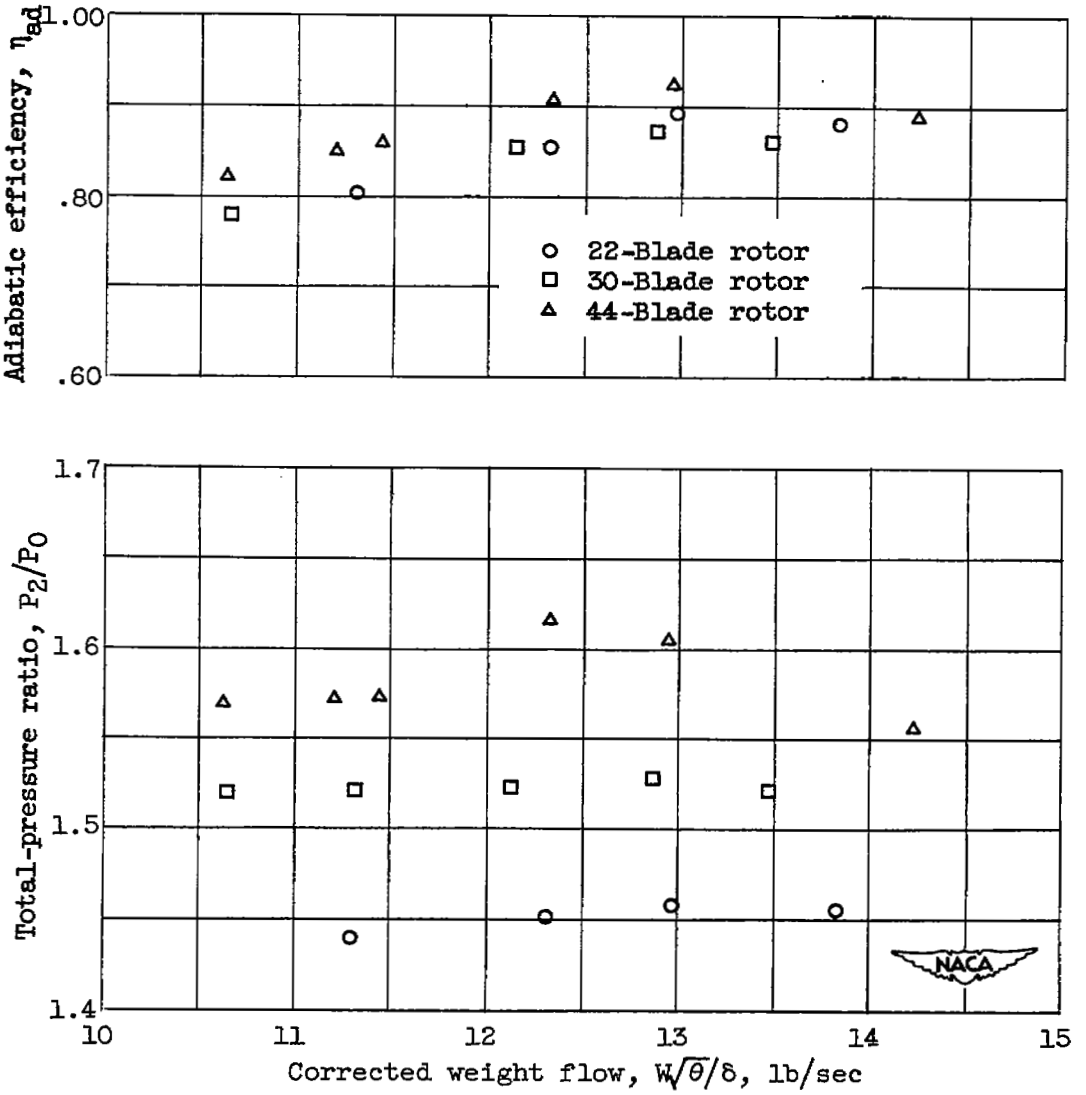

(e) Equivalent tip speed, 962 feet per second.

Figure 4. - Concluded. Variation of total-pressure ratio and adiabatic efficiency with corrected weight flow.

[redacted]

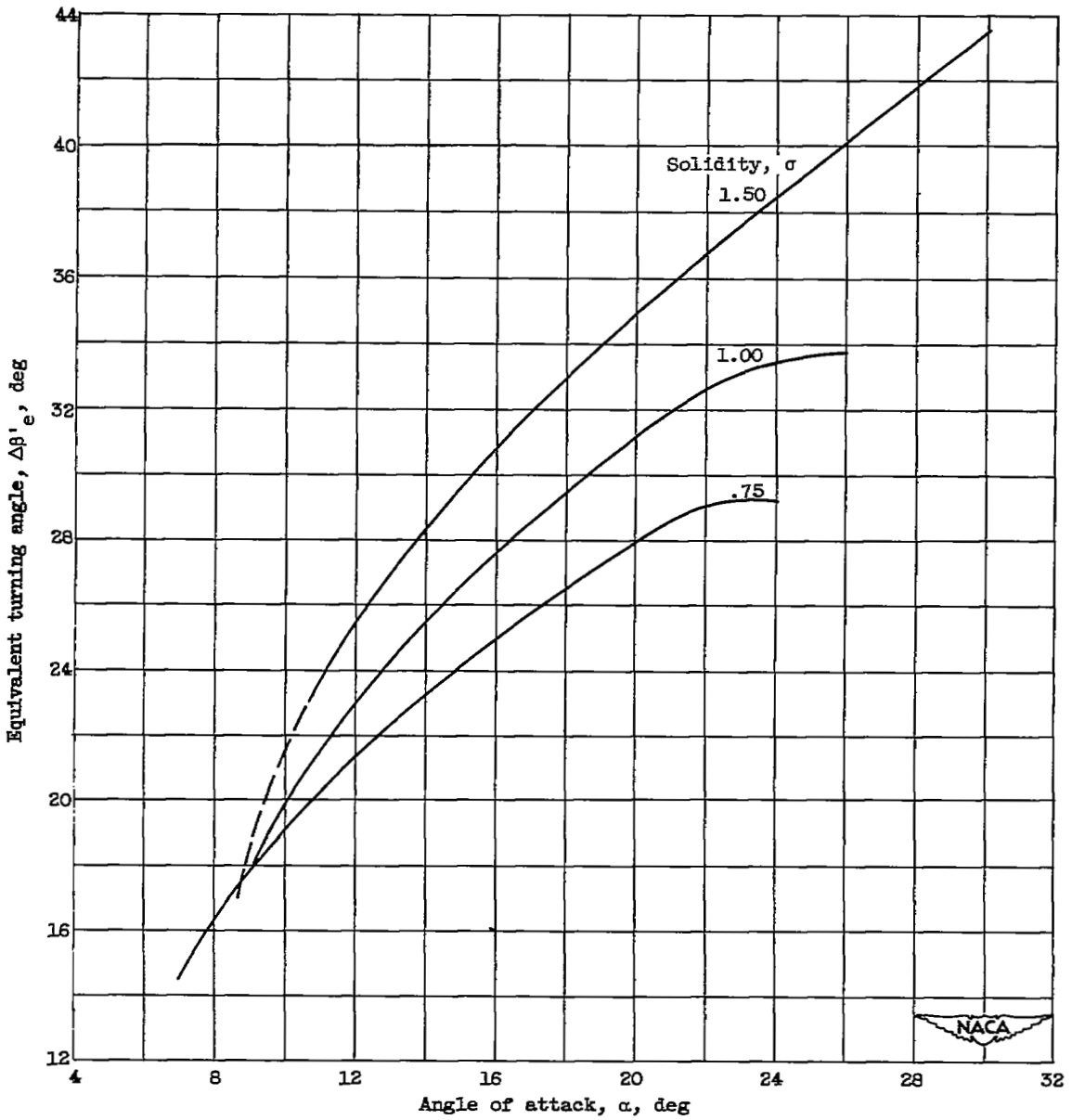

Figure 5. - Variation of turning angle with angle of attack at constant inlet stagger angle for NACA 65-(18)10 airfoil. Equivalent stagger angle $\beta'_{e,1}$, 45°.

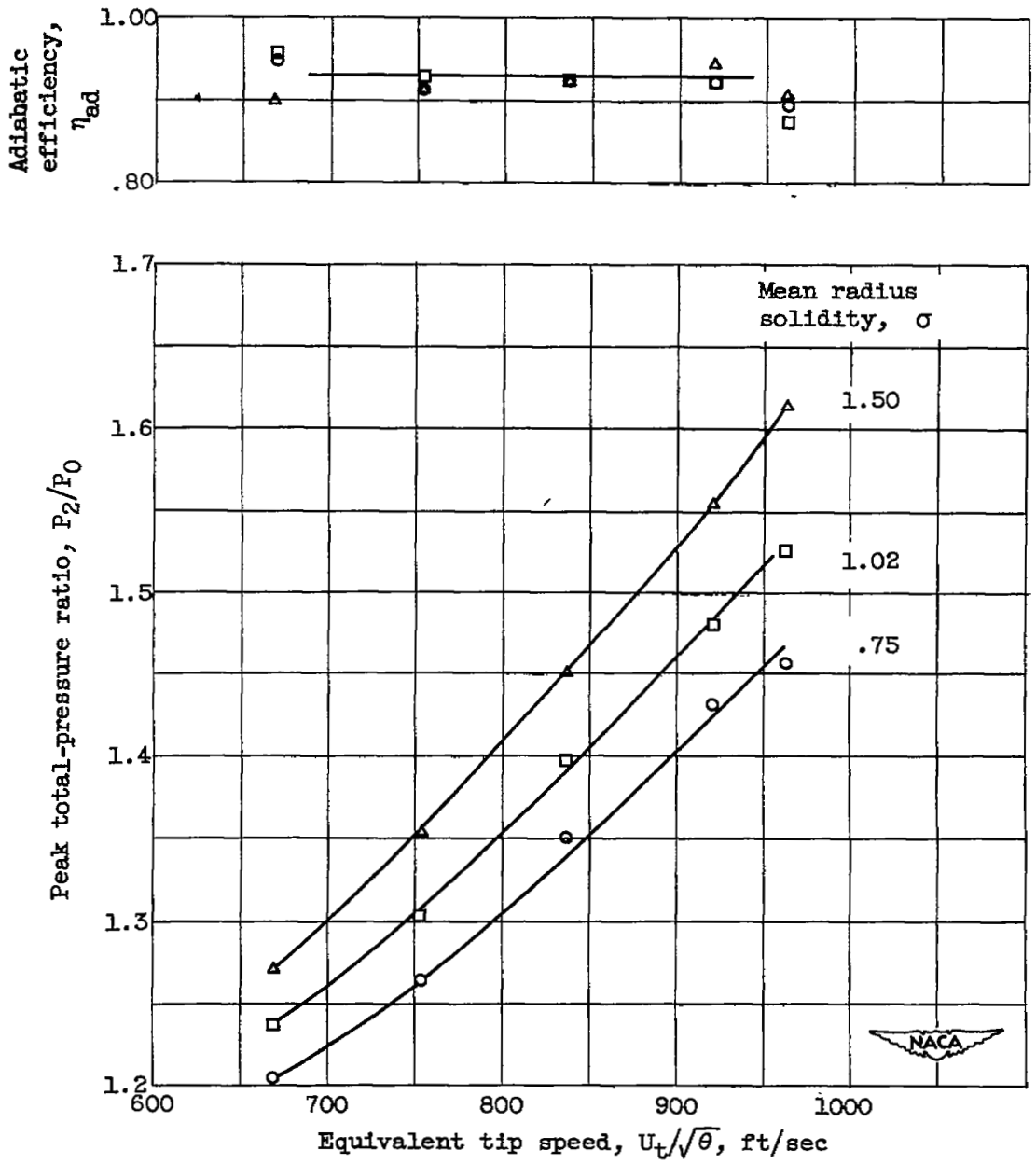

Figure 6. - Variation of peak pressure ratio and corresponding adiabatic efficiency with equivalent tip speed.

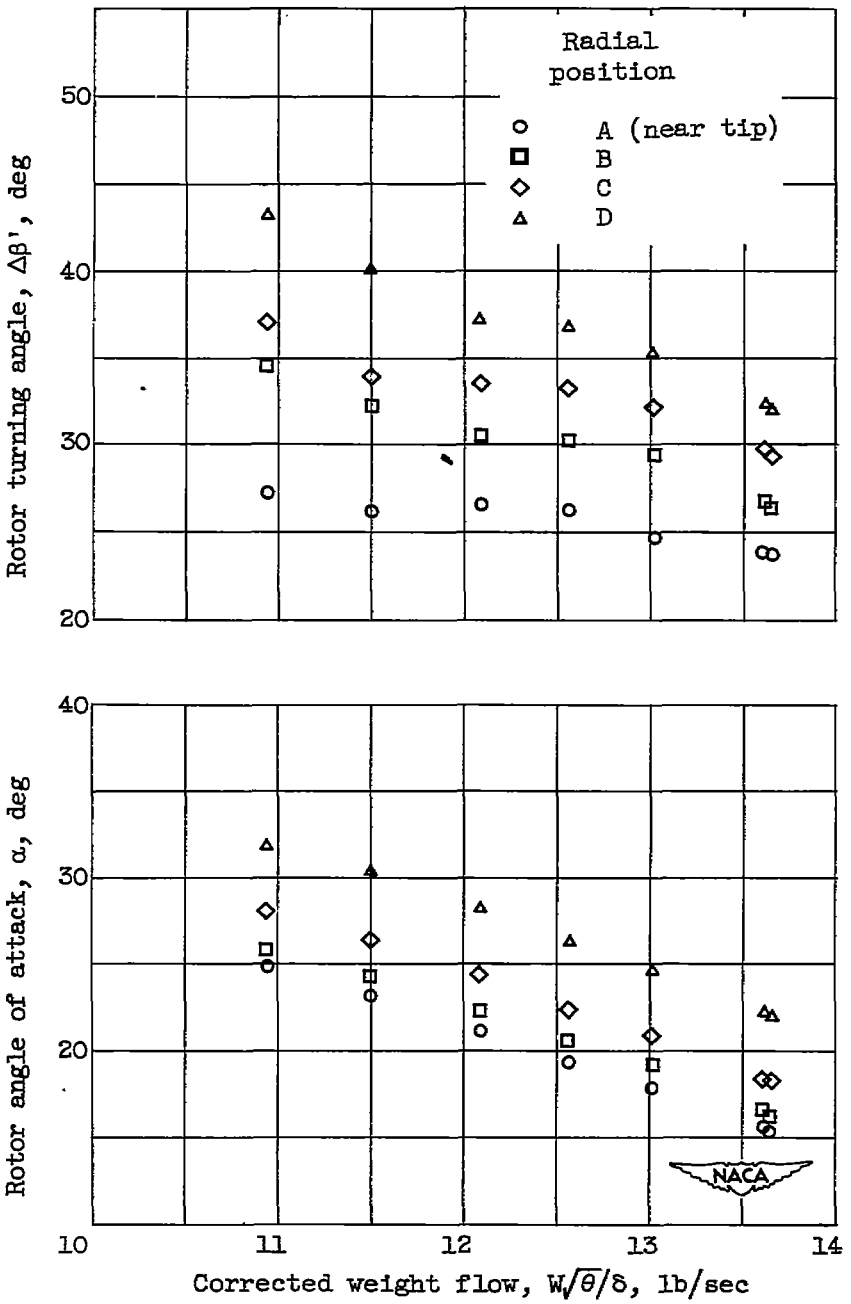

(a) High solidity.

Figure 7. - Variation of rotor angle of attack and turning angle at four radial positions with corrected weight flow. Equivalent tip speed, 836 feet per second.

[redacted]

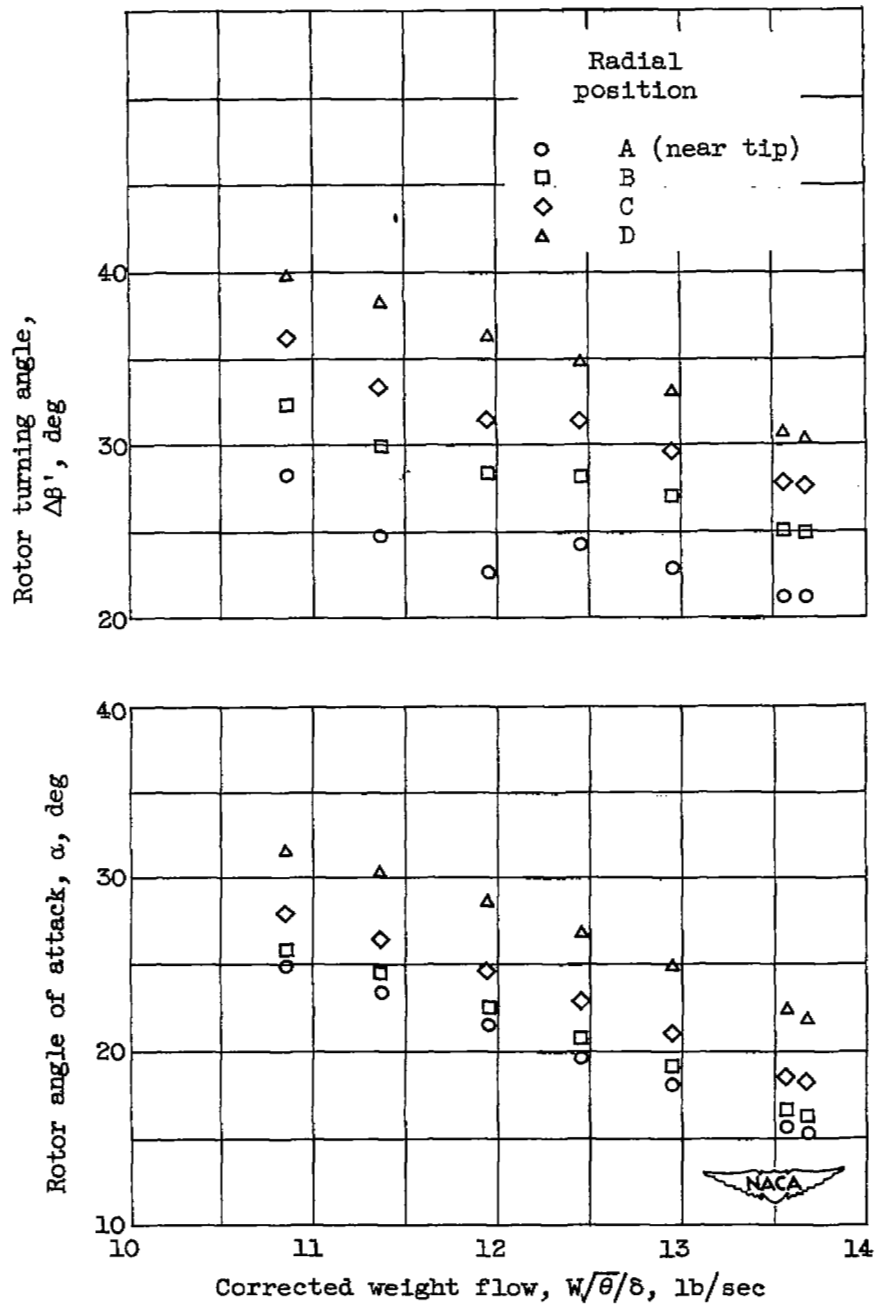

(b) Medium solidity.

Figure 7. - Continued. Variation of rotor angle of attack and turning angle at four radial positions with corrected weight flow. Equivalent tip speed, 836 feet per second.

[redacted]

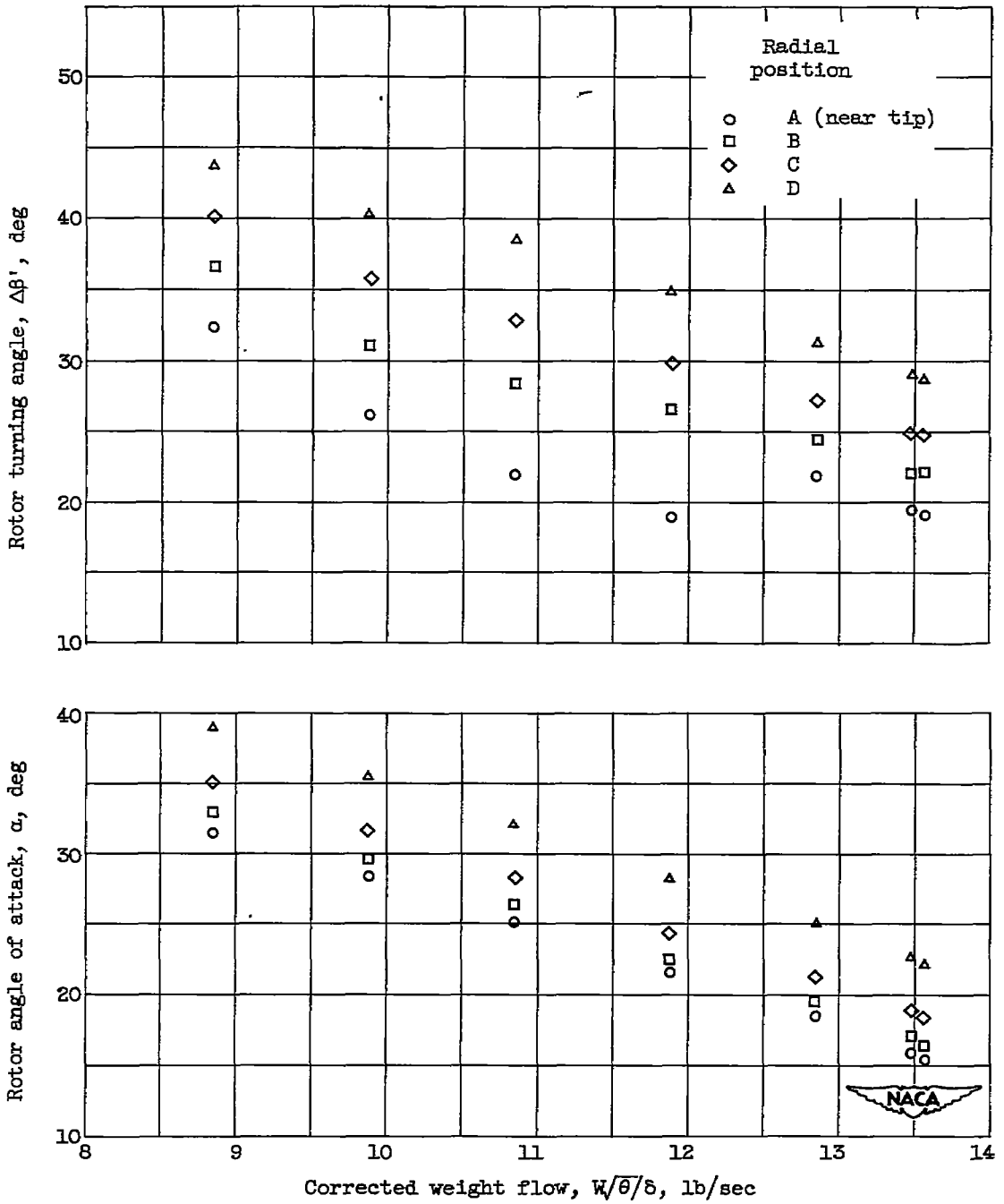

(c) Low solidity.

Figure 7. - Concluded. Variation of rotor angle of attack and turning angle at four radial positions with corrected weight flow. Equivalent tip speed, 836 feet per second.

[redacted]

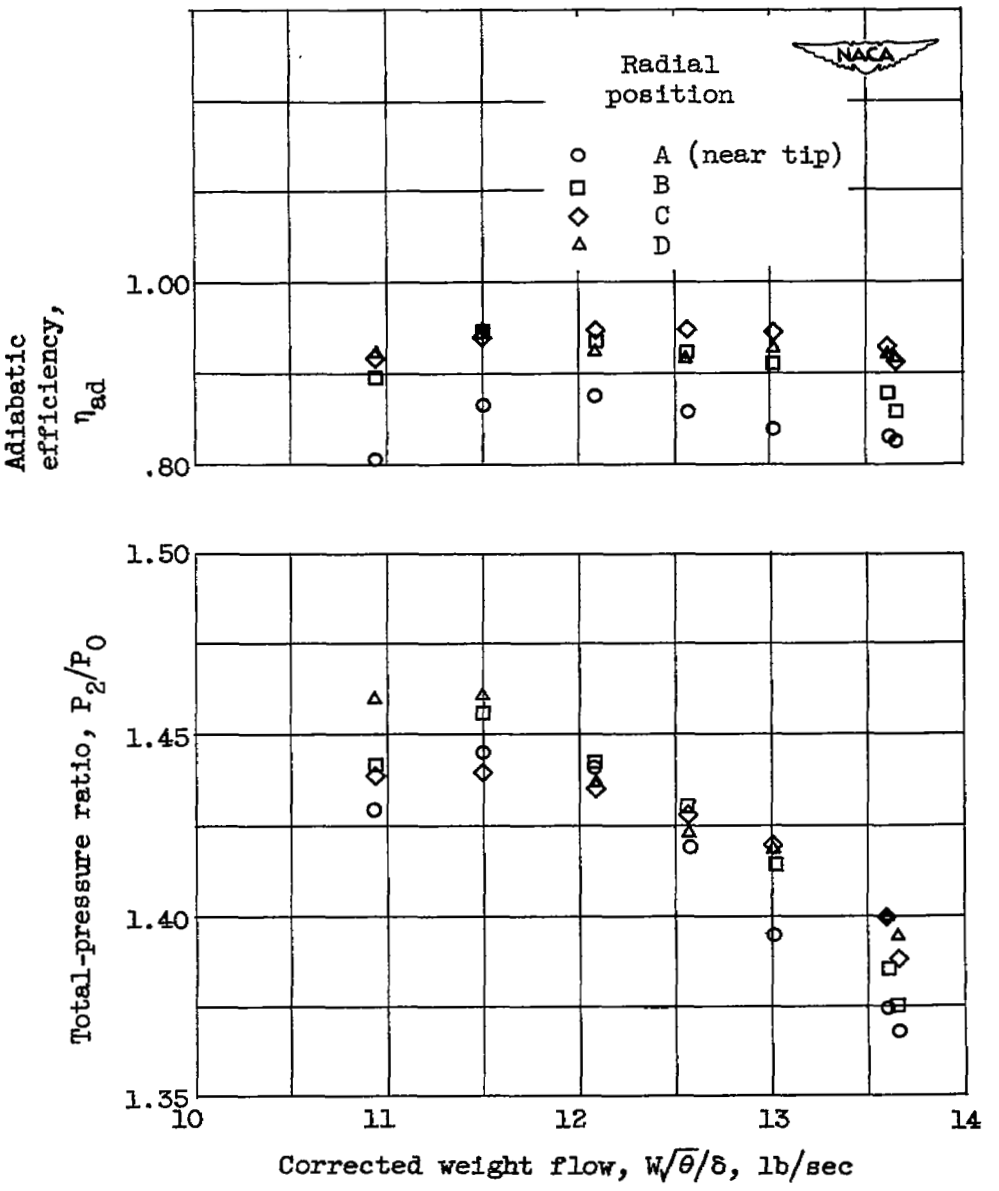

(a) High solidity.

Figure 8. - Variation of total-pressure ratio and adiabatic efficiency at four radial positions with corrected weight flow. Equivalent tip speed, 836 feet per second.

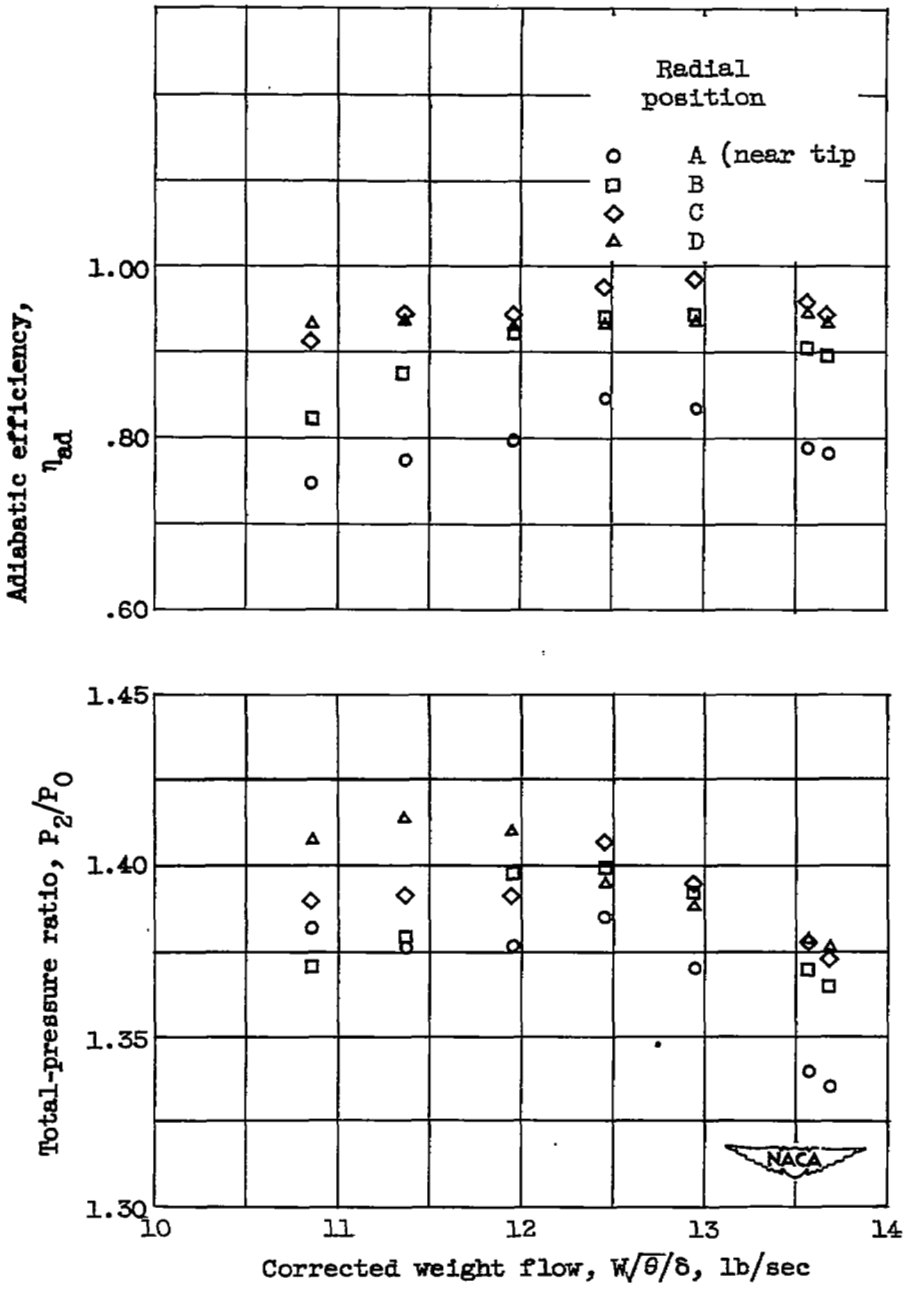

(b) Medium solidity.

Figure 8. - Continued. Variation of total-pressure ratio and adiabatic efficiency at four radial positions with corrected weight flow. Equivalent tip speed, 836 feet per second.

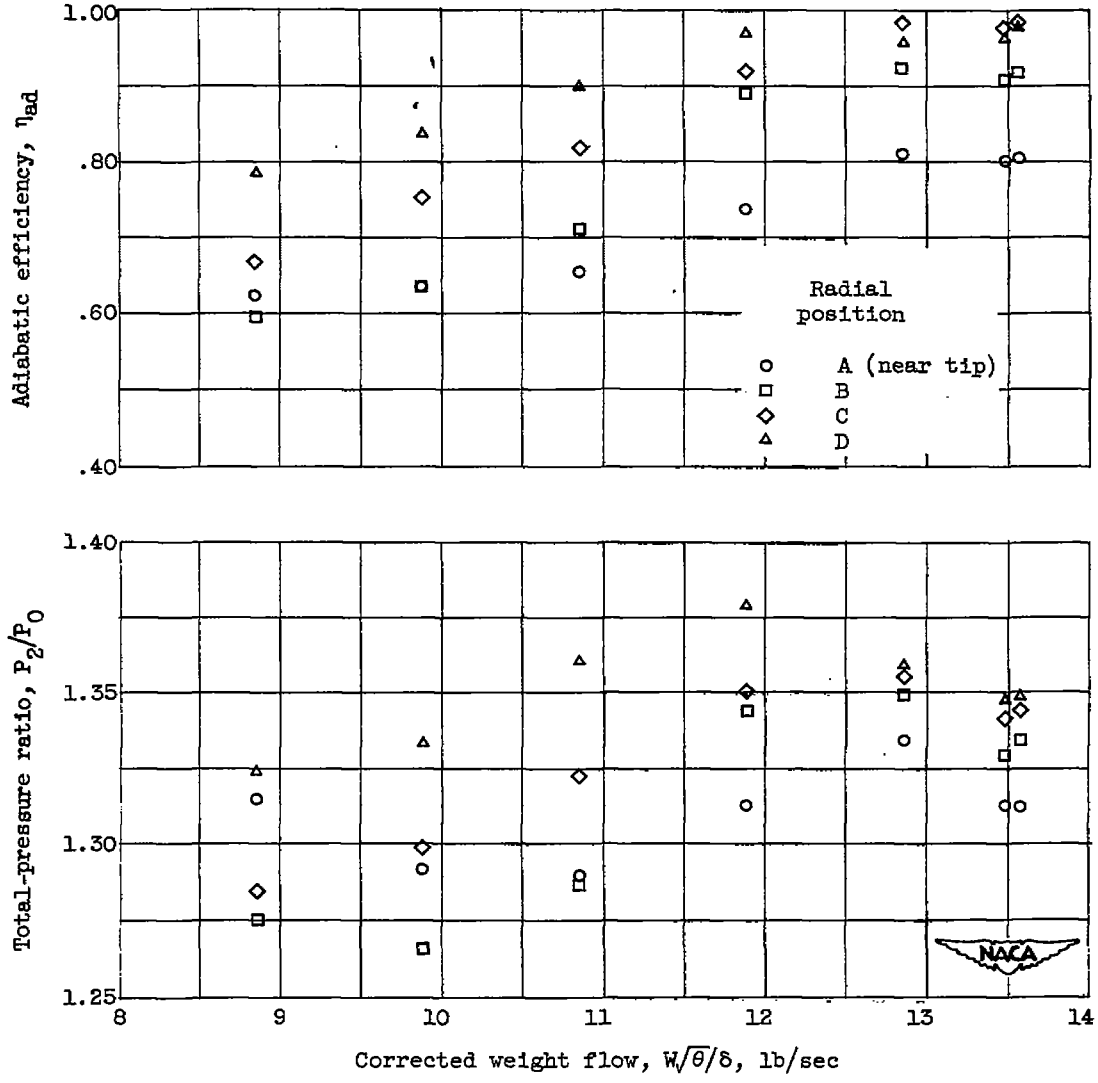

(c) Low solidity.

Figure 8. - Concluded. Variation of total-pressure ratio and adiabatic efficiency at four radial positions with corrected weight flow. Equivalent tip speed, 836 feet per second.

[redacted]

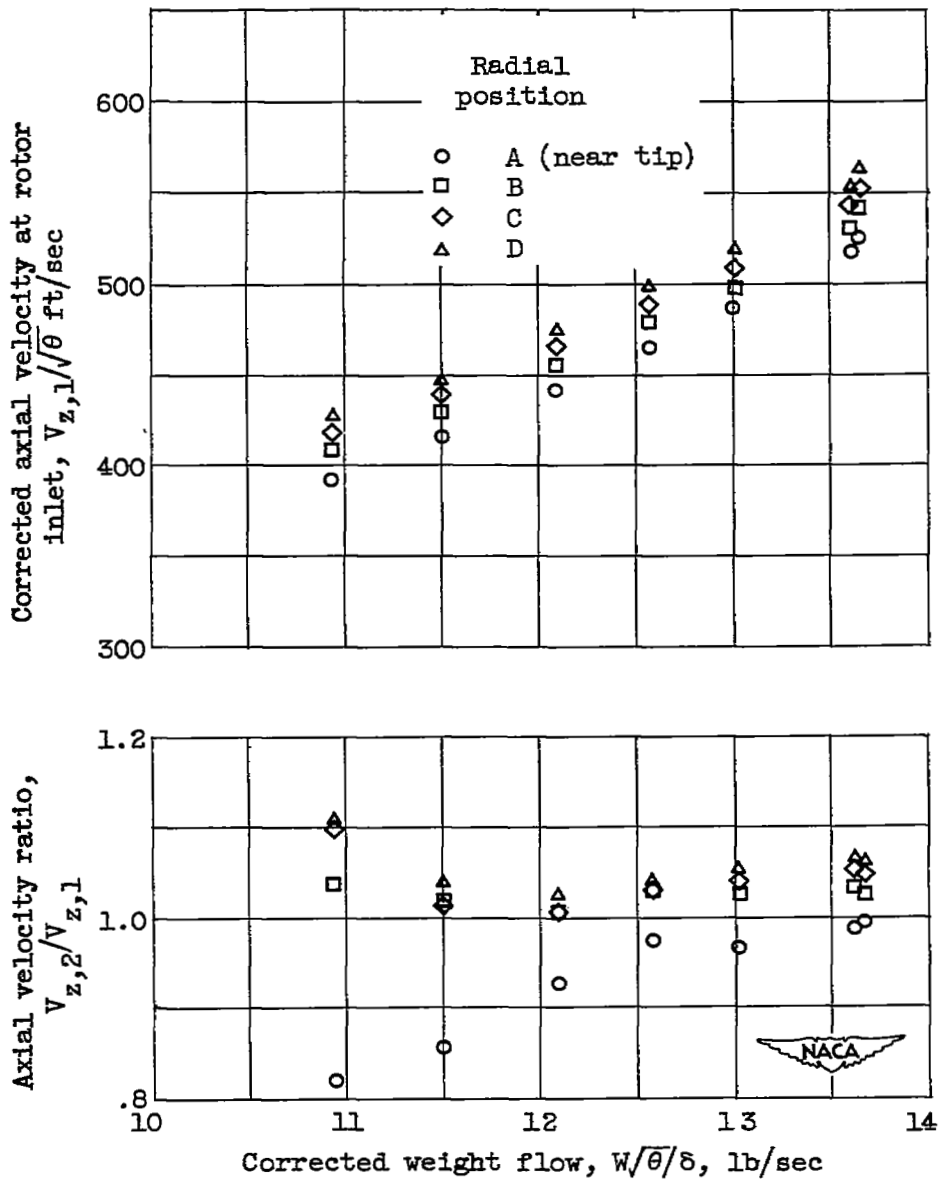

(a) High solidity.

Figure 9. - Variation of corrected axial velocity at rotor inlet and axial velocity ratio at four radial positions with corrected weight flow. Equivalent tip speed, 836 feet per second.

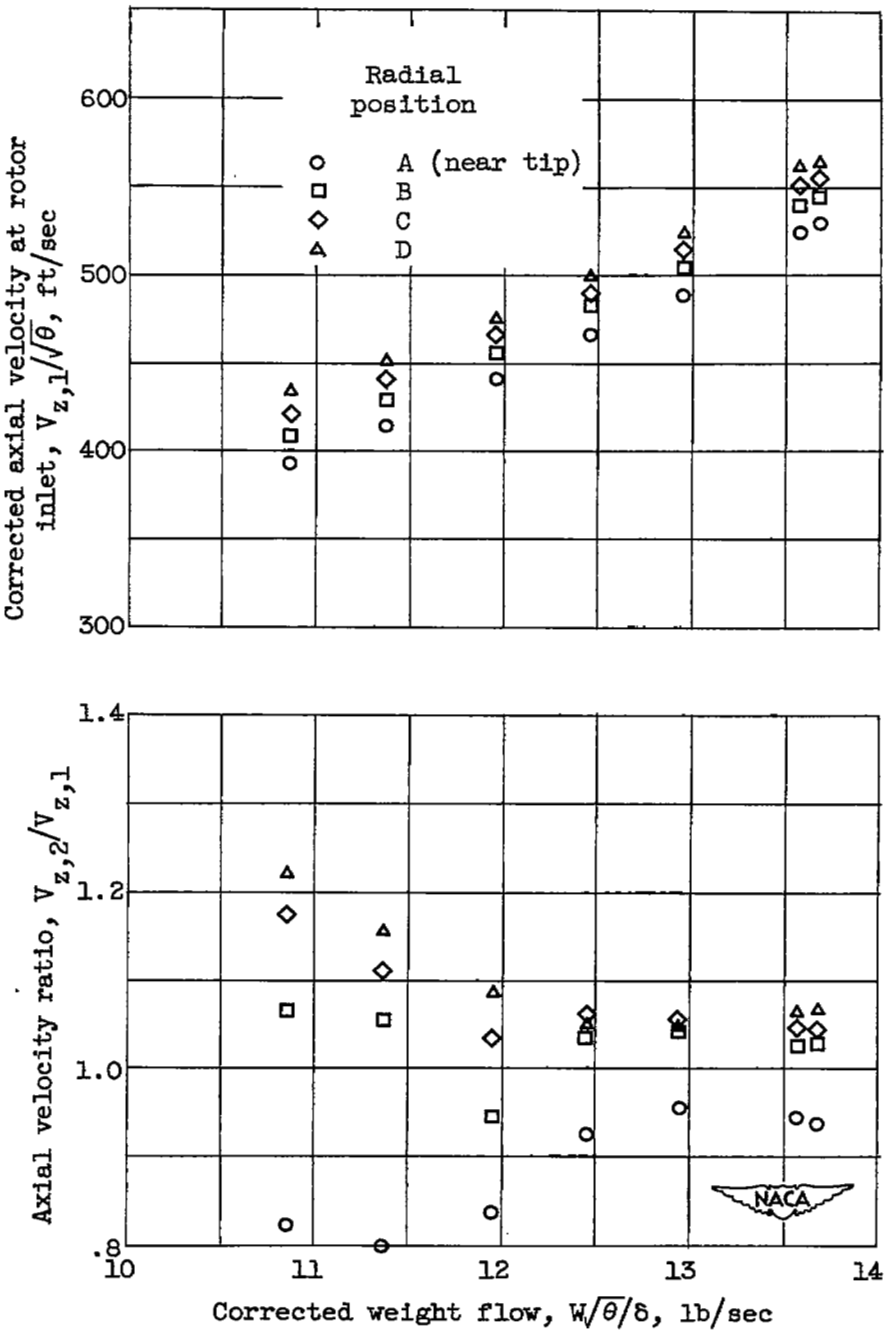

(b) Medium solidity.

Figure 9. - Continued. Variation of corrected axial velocity at rotor inlet and axial velocity ratio at four radial positions with corrected weight flow. Equivalent tip speed, 836 feet per second.

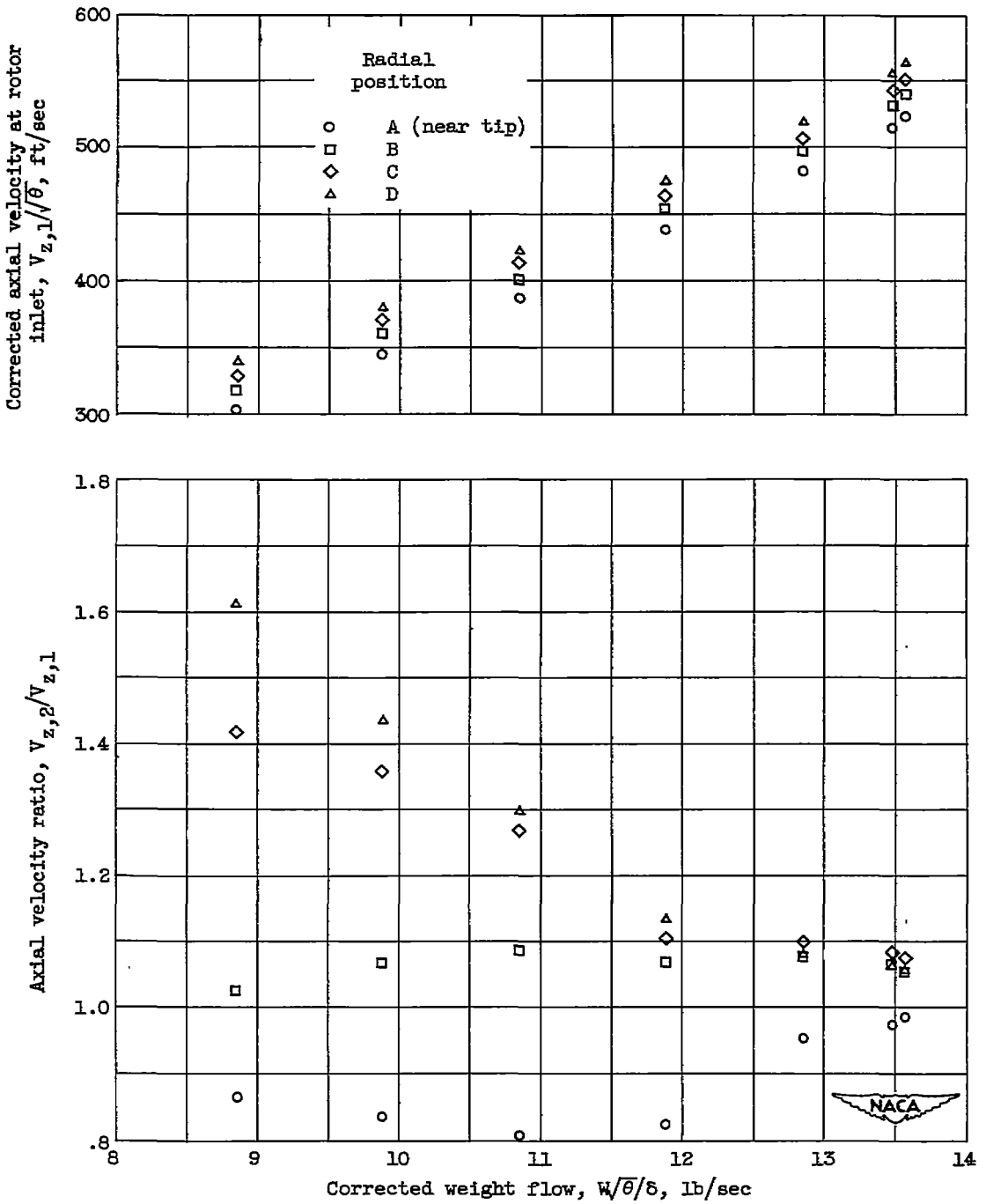

(c) Low solidity.

Figure 9. - Concluded. Variation of corrected axial velocity at rotor inlet and axial velocity ratio at four radial positions with corrected weight flow. Equivalent tip speed, 836 feet per second.

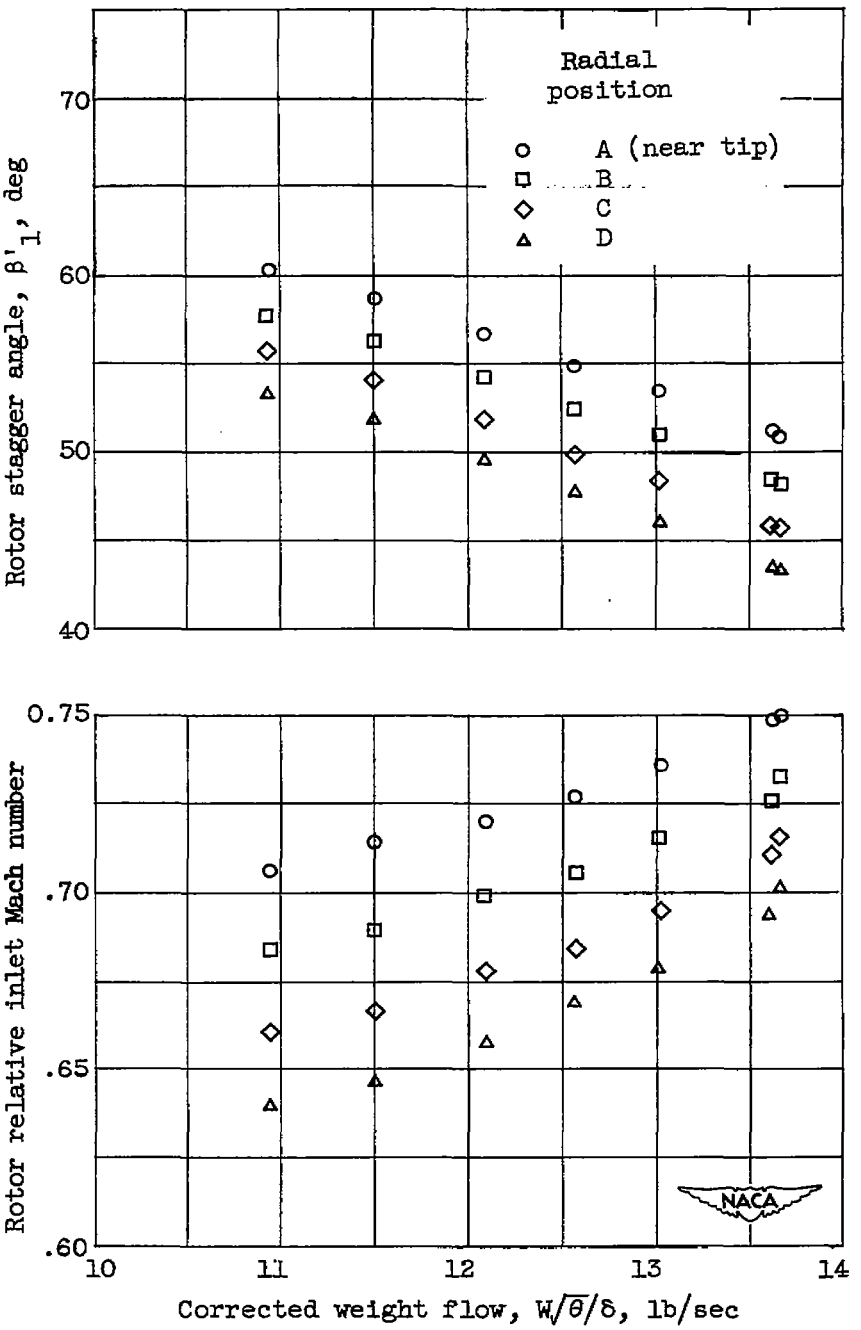

(a) High solidity.

Figure 10. - Variation of rotor stagger angle and relative inlet Mach number at four radial positions with corrected weight flow. Equivalent tip speed, 836 feet per second.

[redacted]

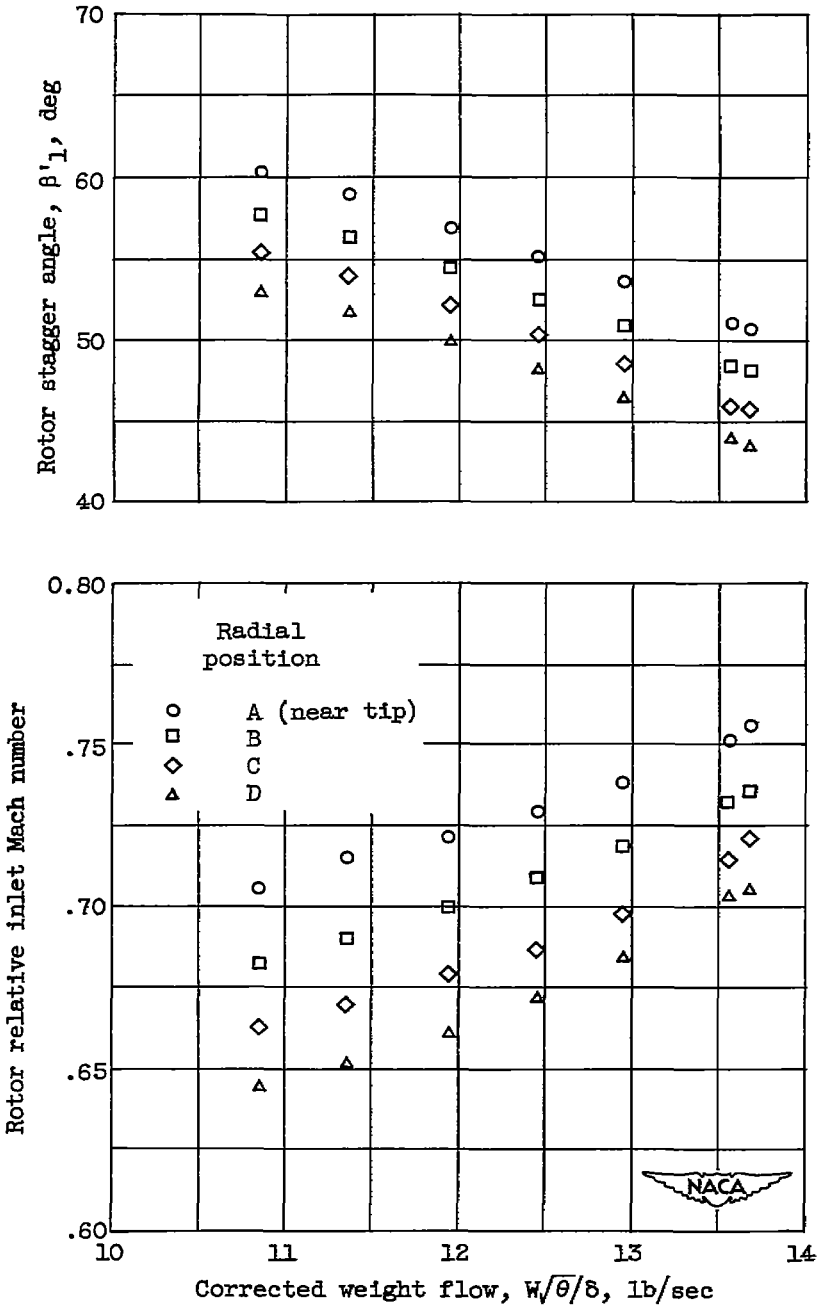

(b) Medium solidity.

Figure 10. - Continued. Variation of rotor stagger angle and relative inlet Mach number at four radial positions with corrected weight flow. Equivalent tip speed, 836 feet per second.

[redacted]

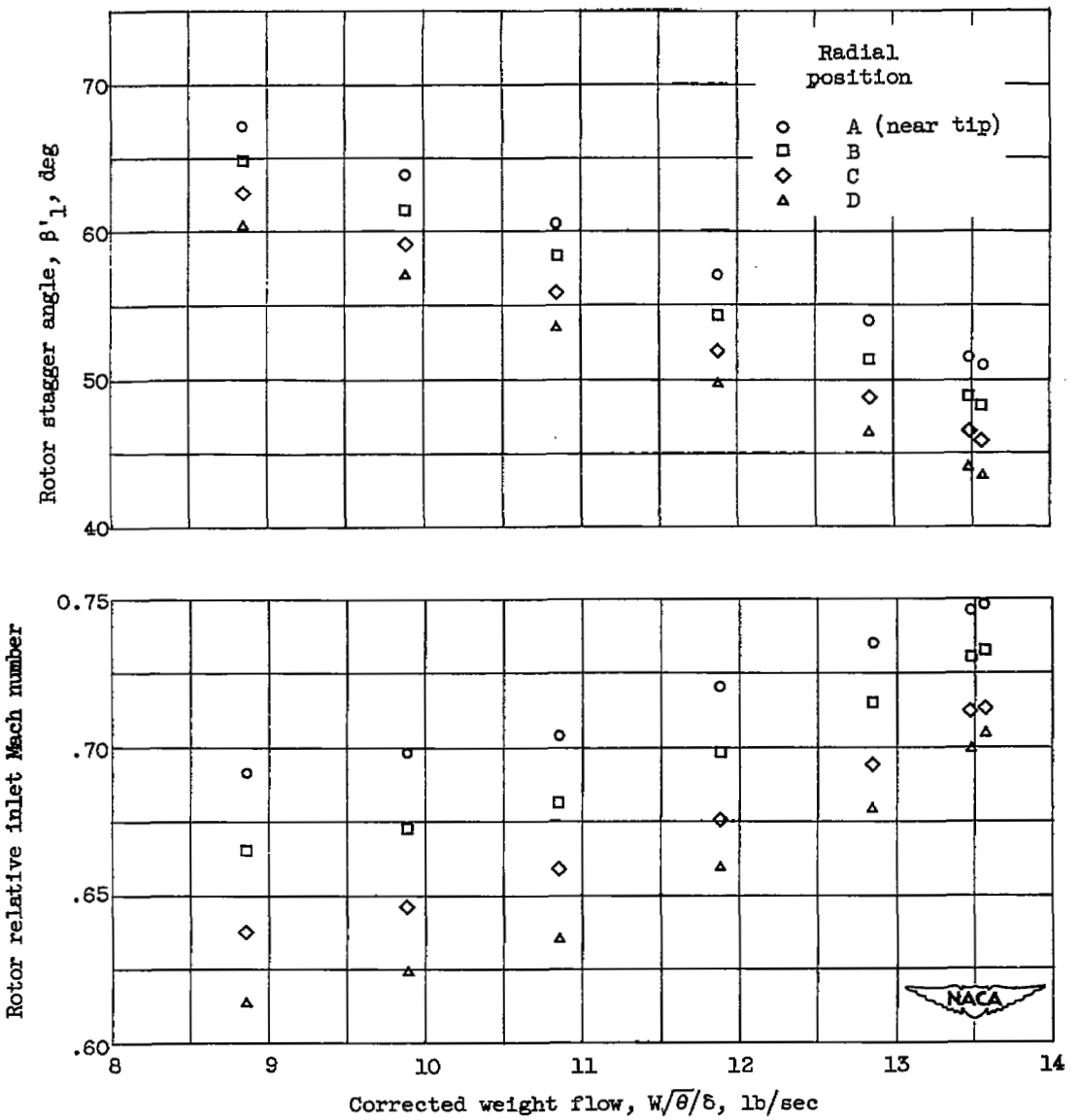

(c) Low solidity.

Figure 10. - Concluded. Variation of rotor stagger angle and relative inlet Mach number at four radial positions with corrected weight flow. Equivalent tip speed, 836 feet per second.

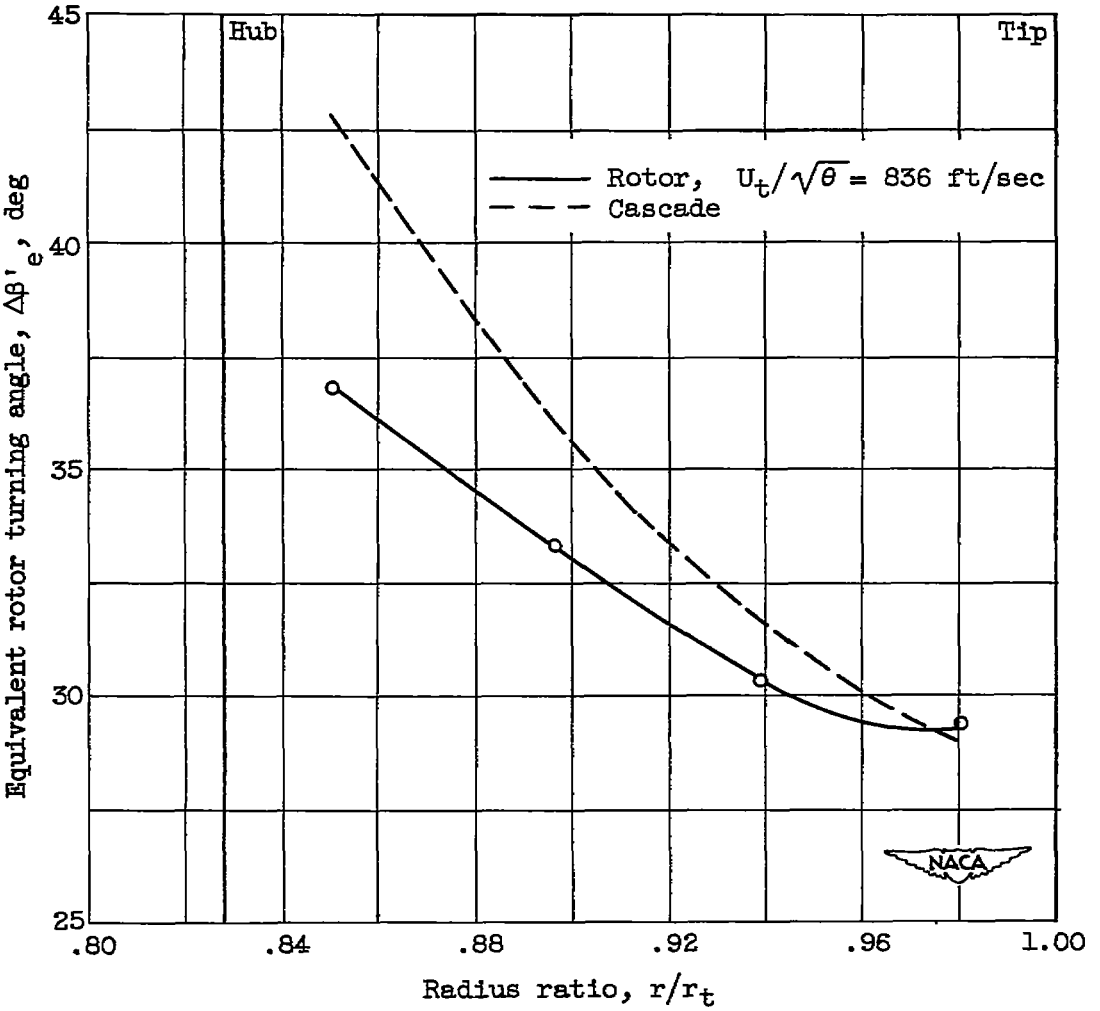

(a) High solidity.

Figure 11. - Comparison of rotor turning angles at various radii with two-dimensional cascade results.

[redacted]

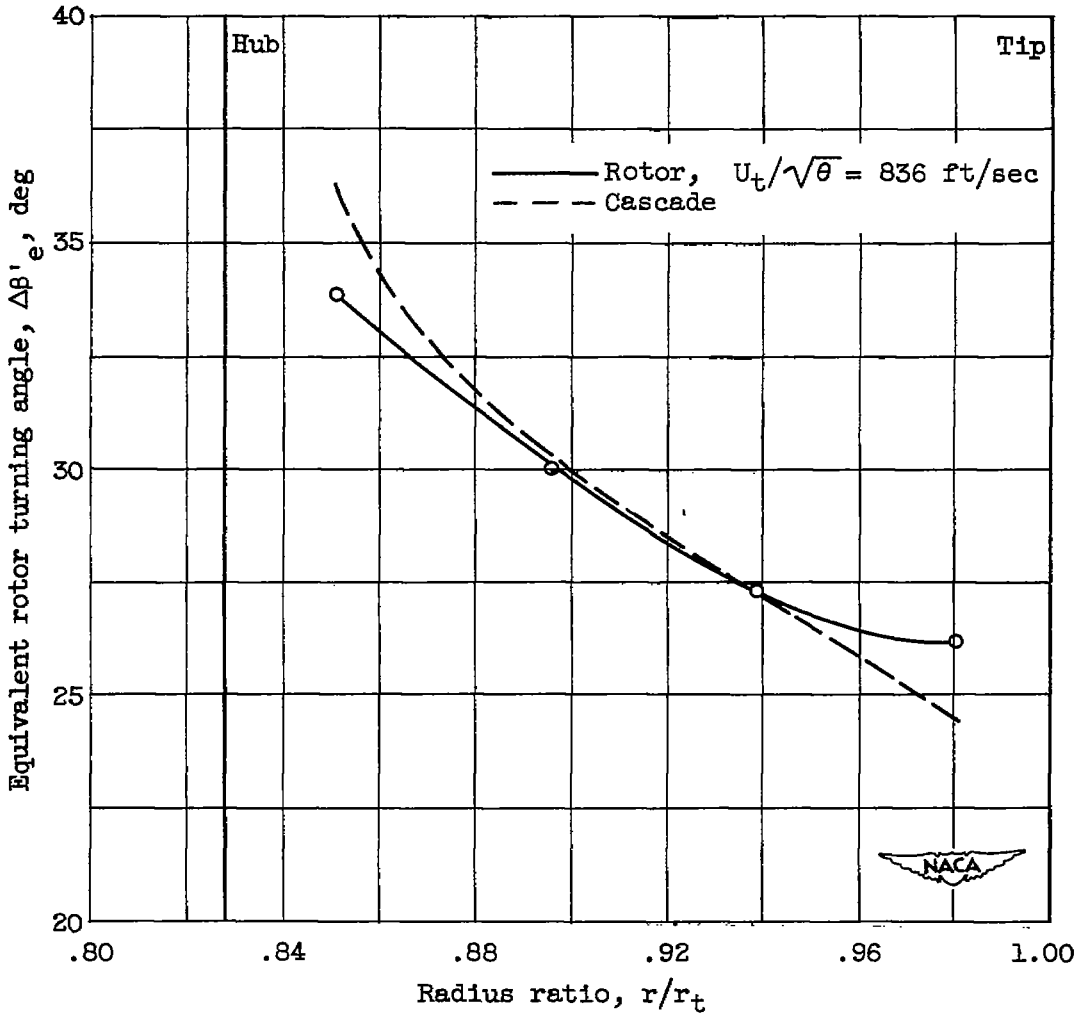

(b) Medium solidity.

Figure 11. - Continued. Comparison of rotor turning angles at various radii with two-dimensional cascade results.

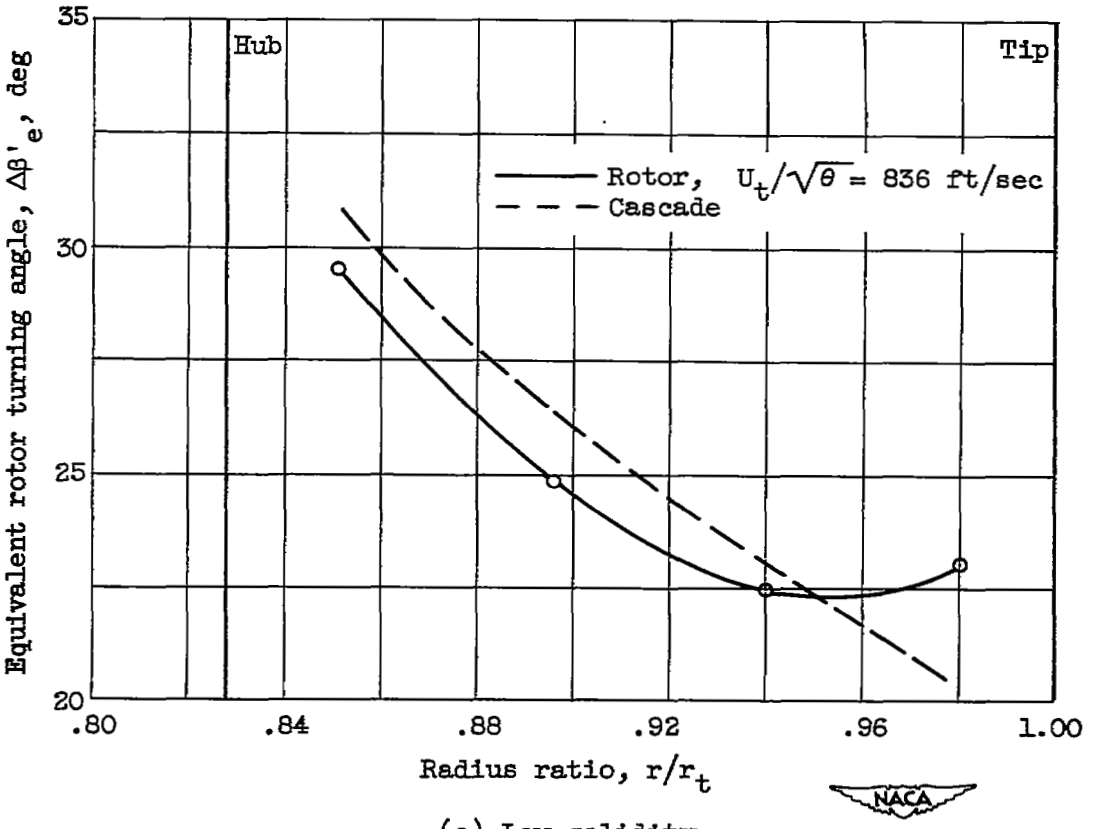

(c) Low solidity.

Figure 11. - Concluded. Comparison of rotor turning angles at various radii with two-dimensional cascade results.

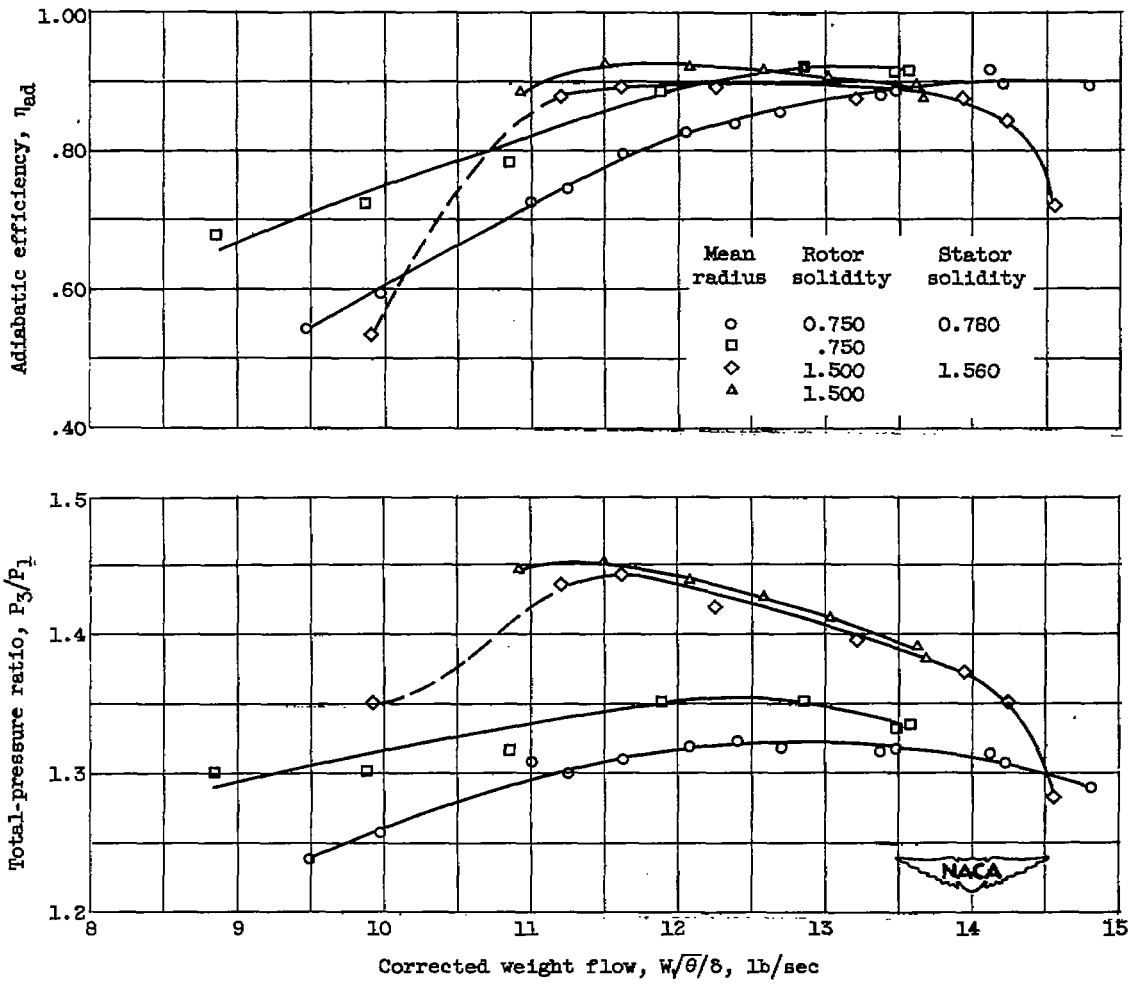

Figure 12. - Variation of total-pressure ratio and adiabatic efficiency for complete compressor stage with corrected weight flow. Equivalent tip speed, 836 feet per second.

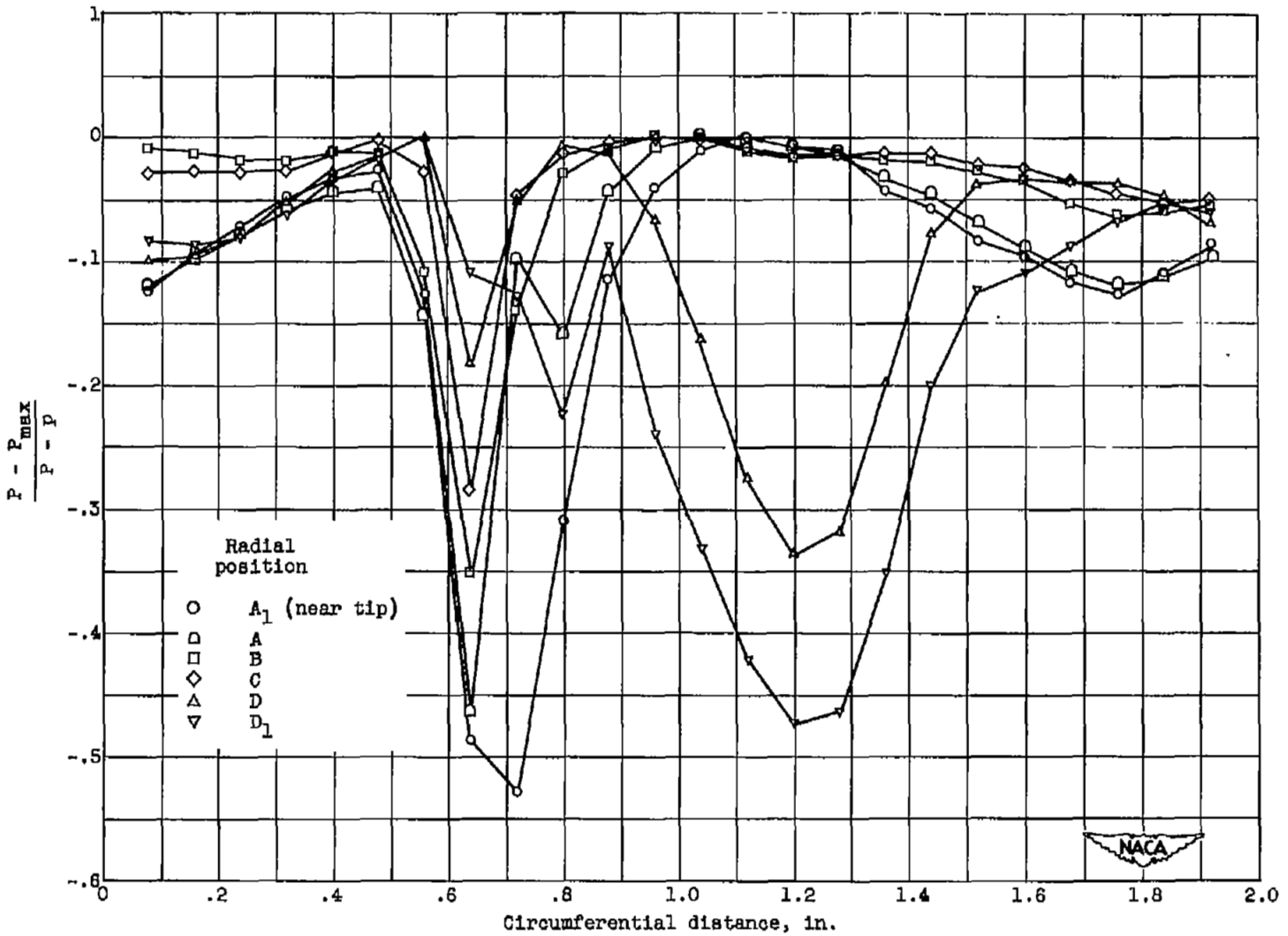

(a) Corrected weight flow, 14.1 pounds per second.

Figure 13. - Wake survey after low-solidity stator blades. Equivalent tip speed, 836 feet per second.

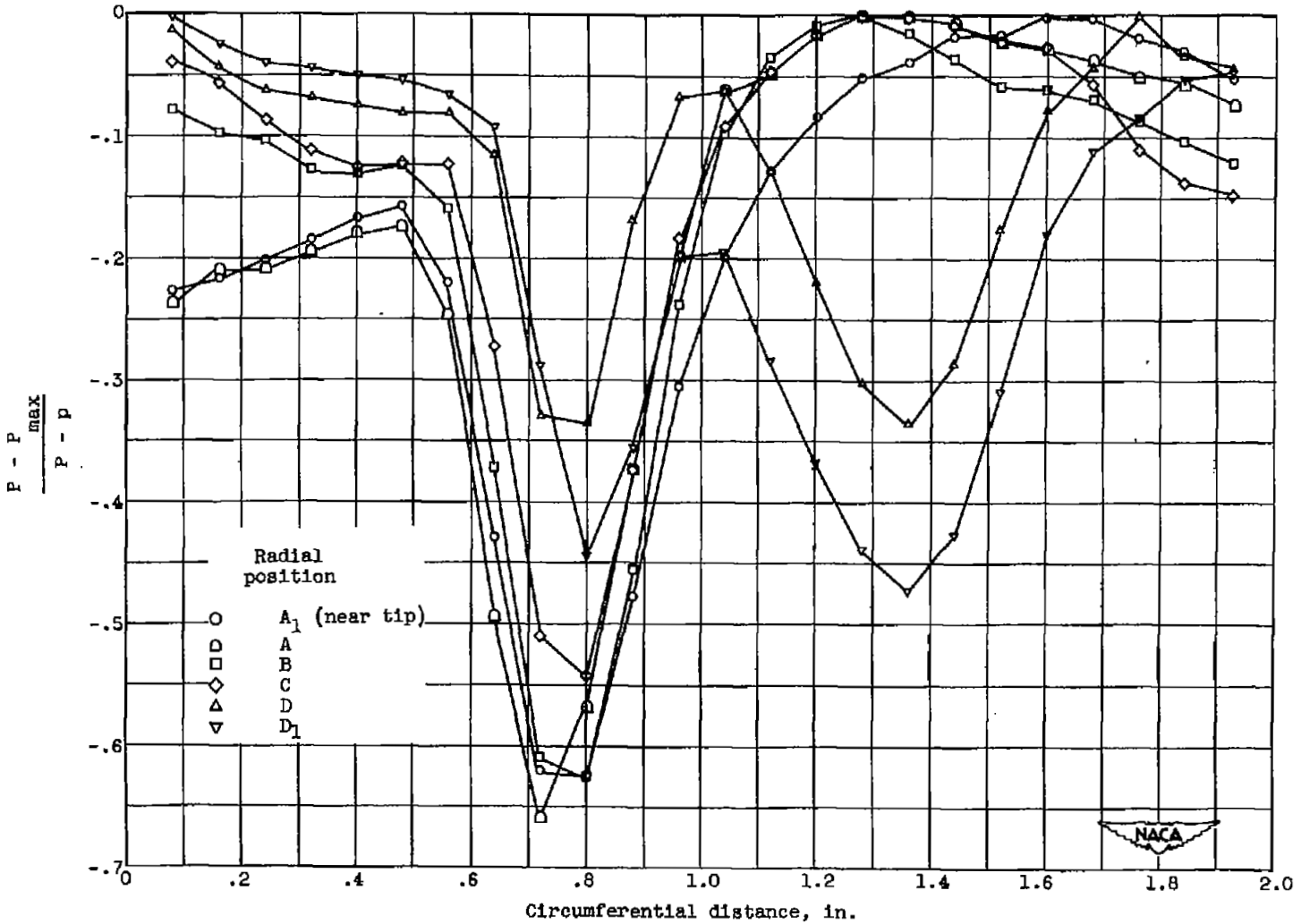

(b) Corrected weight flow, 12.4 pounds per second.

Figure 13. - Continued. Wake survey after low-solidity stator blades. Equivalent tip speed, 836 feet per second.

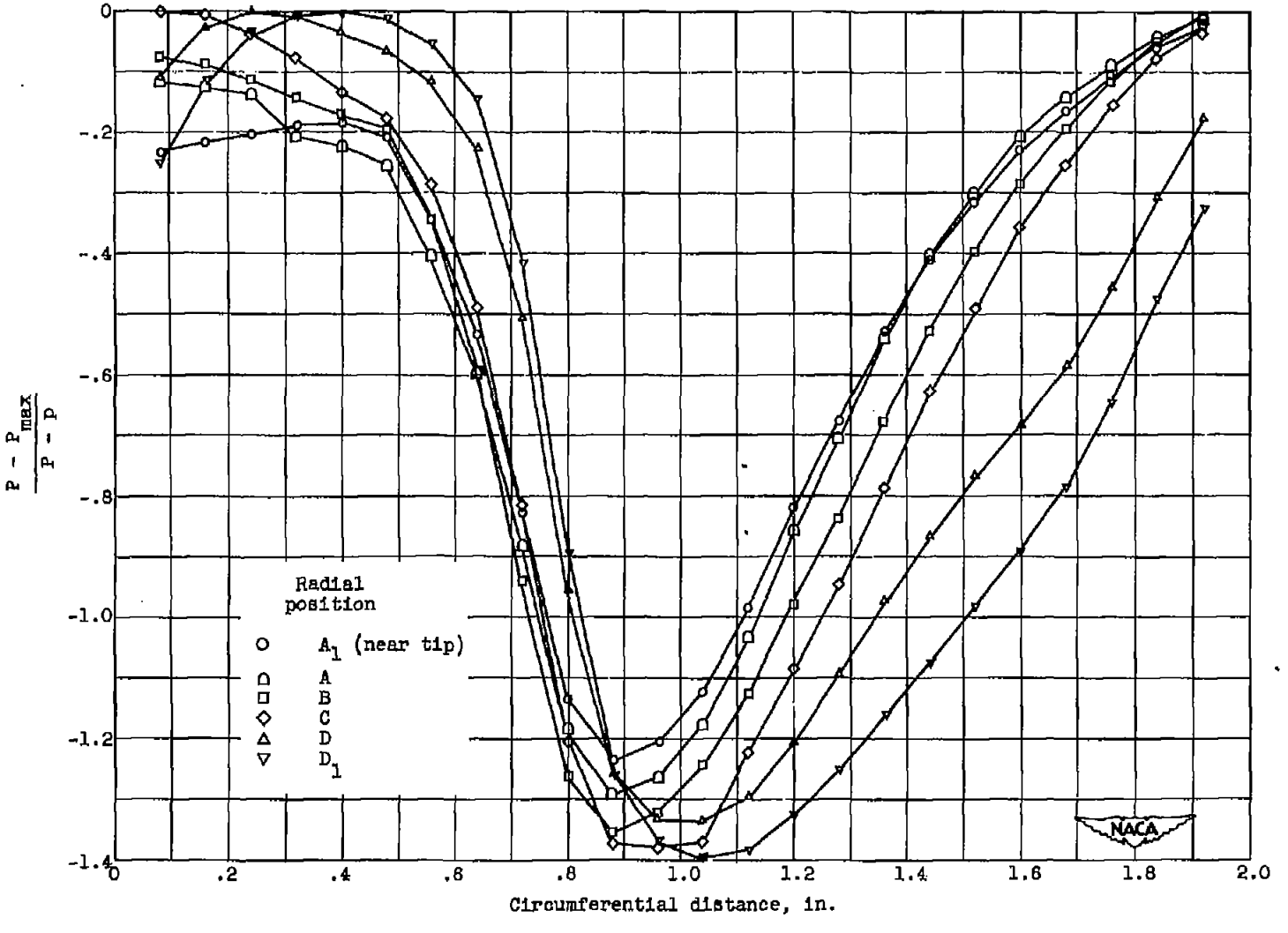

(c) Corrected weight flow, 10.0 pounds per second.

Figure 13. - Concluded. Wake survey after low-solidity stator blades. Equivalent tip speed, 836 feet per second.

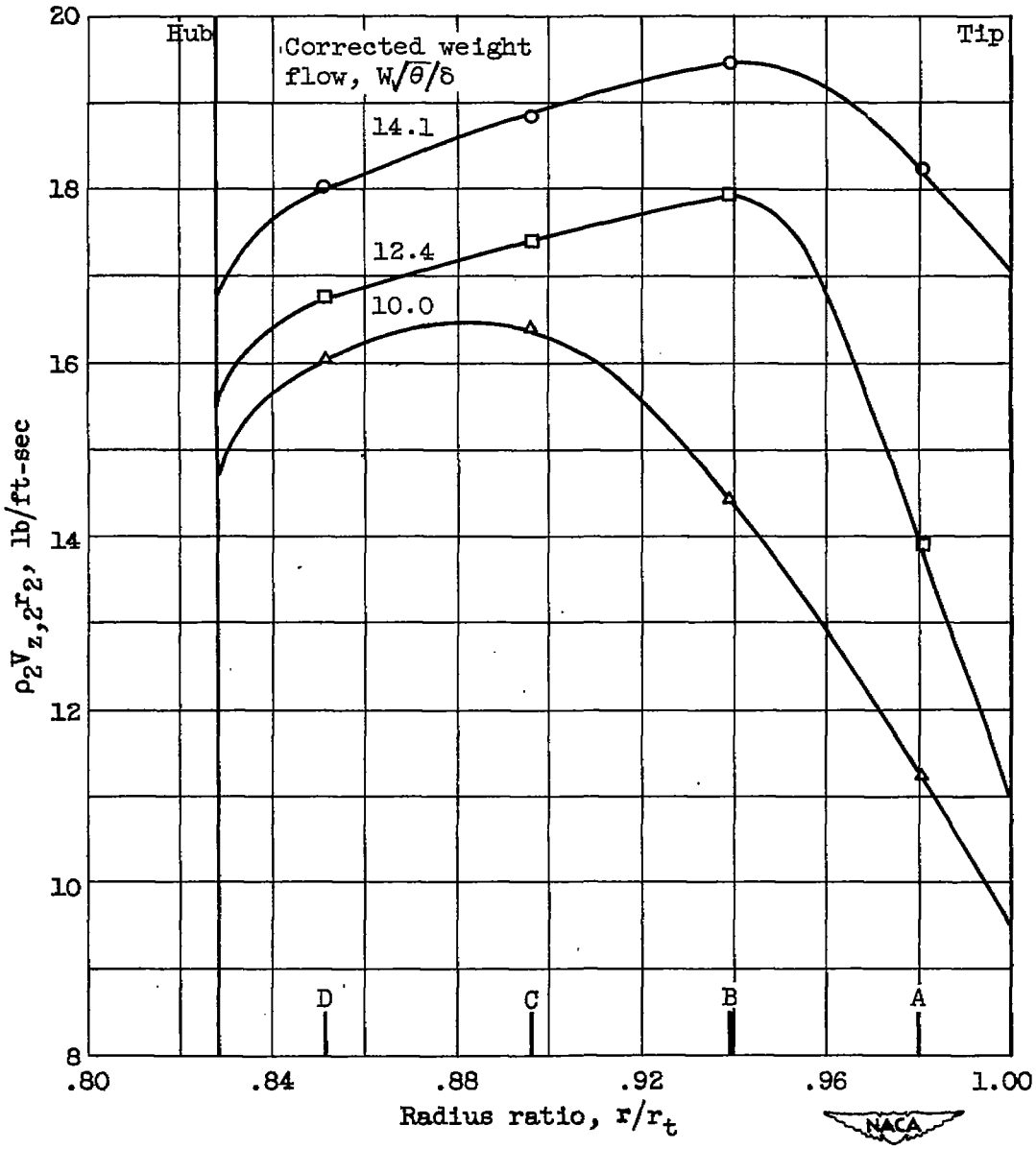

Figure 14. - Flow distribution before low-solidity stator blades. Equivalent tip speed, 836 feet per second.

[redacted]

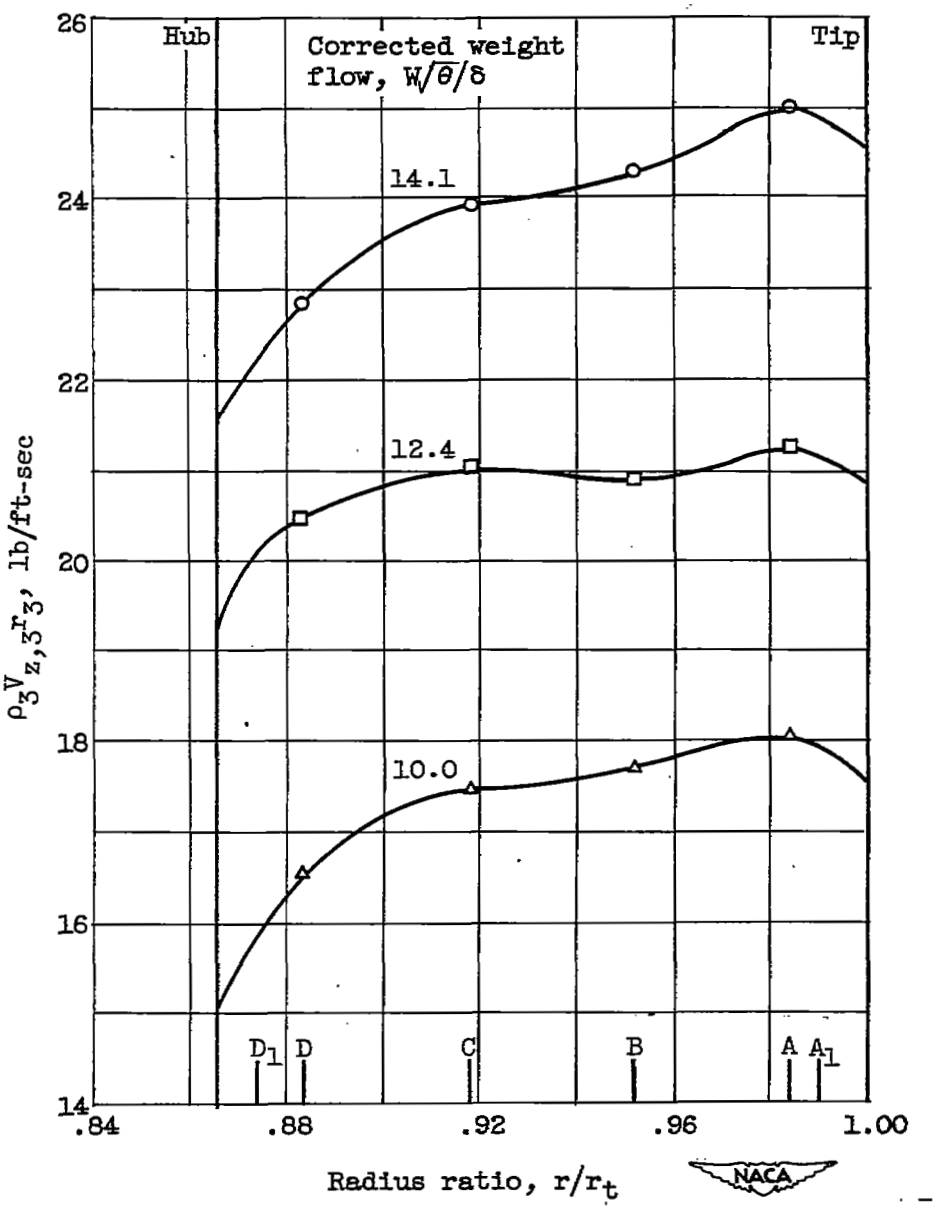

Figure 15. - Flow distribution after low-solidity stator blades. Equivalent tip speed, 836 feet per second.

[redacted]

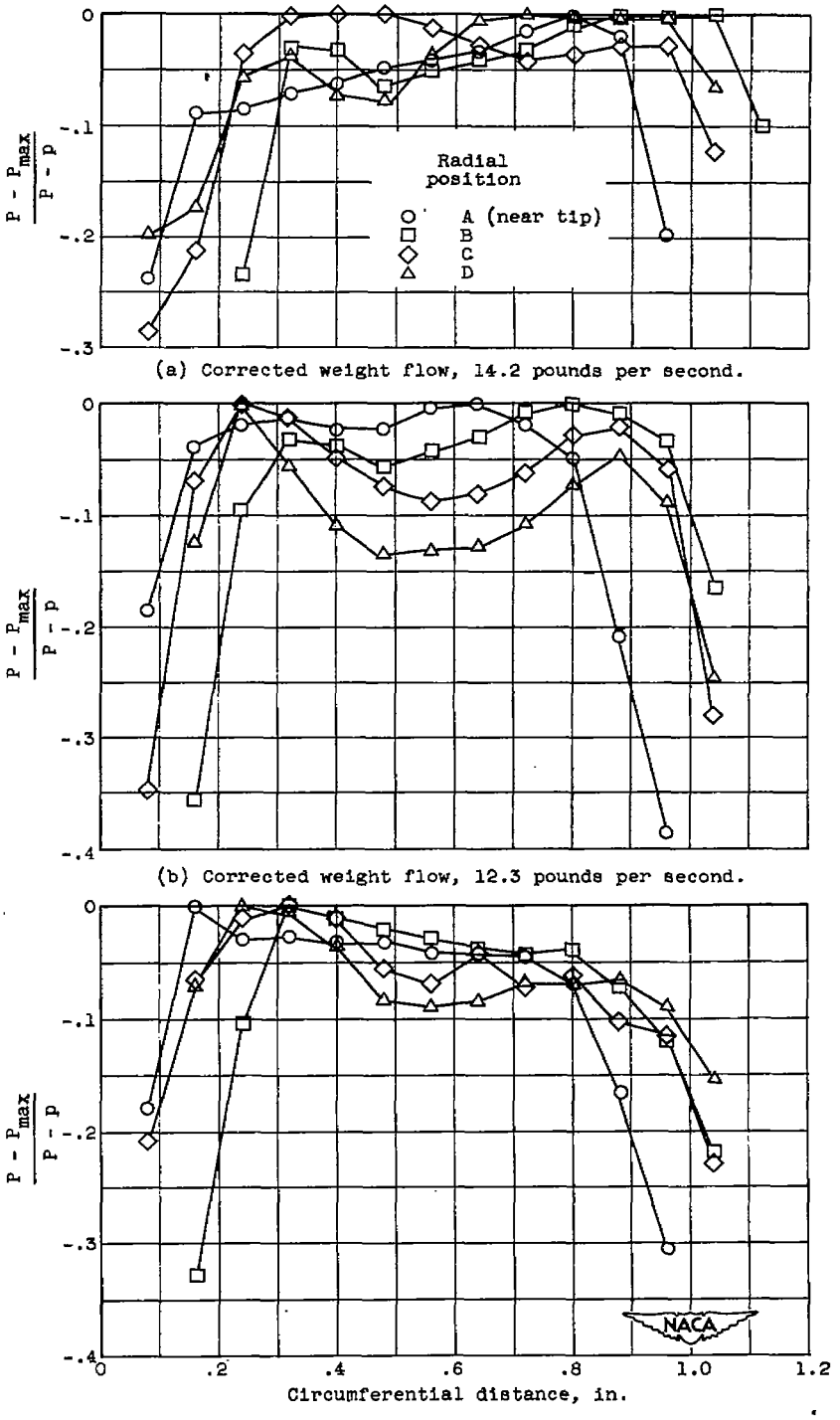

Figure 16. - Wake survey after high-solidity stator blades. Equivalent tip speed, 836 feet per second.

[redacted]

NACA-Langley - 4-14-52 - 375